Coupled triads in the dynamics of internal waves: Case study using a linearly stratified fluid

Q. Pan,[1,*] N. N. Peng,[1] H. N. Chan,[2] and K. W. Chow[1]
[1]*Department of Mechanical Engineering, University of Hong Kong, Pokfulam, Hong Kong*
[2]*Department of Mathematics, Chinese University of Hong Kong, Shatin, New Territories, Hong Kong*

(Received 7 May 2020; accepted 21 January 2021; published 22 February 2021)

In a linearly stratified fluid, two sets of resonant triads with one member in common, hence coupled, can arise for a wide range of wave numbers where all five waves travel in the same direction. The nonlinear dynamics is investigated by deriving the evolution equations of slowly varying wave packets. The dependence of the interaction coefficients on the channel depth and the buoyancy frequency are explicitly demonstrated. Coupling may produce instabilities with growth rates bigger than those displayed by either triad in isolation. Similar properties are expected for layered fluids with shear currents. By drawing on a recent link between modulation instability and the occurrence of rogue waves, surprisingly large displacements in the interior of the fluid are thus more likely. For applications to oceanography, the interaction coefficients of the evolution equations will affect the magnitude of the actual amplitude of an internal rogue wave. Computations indicate that displacements much larger than those of surface rogue waves are possible. From a more theoretical perspective of wave resonance through the Madelung representation, special ranges of dynamical phase angles are identified for the existence of time invariants. Finally, numerical simulations of a simplified system are performed to highlight the spontaneous generation of modes due to coupling.

DOI: 10.1103/PhysRevFluids.6.024802

I. INTRODUCTION

Wave interaction can serve as a mechanism in conveying information as well as energy, and as such constitutes a significant factor in the dynamics of surface and internal waves. Triad resonance involving three waves satisfying special constraints in the angular frequencies and wave numbers has been studied intensively [1,2]. Pure gravity waves will not allow such resonance, but incorporation of capillarity will permit these triads to occur. For a two-layer fluid, this resonance can occur among surface and interfacial waves [3]. If linearly stable or unstable modes are permitted, the evolution equations will be slightly modified to account for this energy loss (gain) but the flexibility in choosing the appropriate modes is further enhanced [1,4]. In a linearly stratified ocean, a case of focus in the present study, only linearly stable modes may be allowed. Envelope equations which describe the slow evolution of the wave packets due to resonant interactions are useful tools in studying the dynamics. While these versions of resonance in layered and stratified fluids typically involve modes moving in opposite directions, in special situations all three participating waves can propagate in the same direction [5]. If the fluid is continuously stratified, the choice of participating modes is even wider. A special case of hyperbolic secant buoyancy frequency profile allows analytical solutions [6]. Such resonance can also be demonstrated experimentally [7,8].

*Corresponding author: upanqing@connect.hku.hk

Triad resonance for internal waves has been studied from the perspective of physical oceanography, as a possible explanation for the cascade of energy from large-scale internal tides to motions of a smaller scale [9,10]. Subharmonic resonance, also widely termed as parametric subharmonic instability, where a given wave train or beam generates further trains of half the frequency of the original unit, has generated intense attention [11–13]. Effects of mean flow and rotation, factors of particular relevance in the geophysical context, have been incorporated [14,15]. In addition to connections with hydrodynamic surface and internal waves, review article on triads for a general setting in physics has been given [16].

The focus of the present work will be sets of coupled triads, or more precisely, a pair of triads with a common member. Hence five distinct waves will be participating in the dynamics of evolution. As examples, early works in the literature on coupled triads address the aspects of "explosive" growth and marginally unstable modes from the perspective of plasma physics and atmospheric science [17,18]. In the realm of fluid mechanics, sets of coupled triads have been considered for surface (internal) waves and also stochastically from the viewpoint of a large ensemble of waves via a Hamiltonian approach [19].

The effects of linear or otherwise arbitrary shear currents on properties of surface waves have also been studied extensively [20,21]. From the perspectives of resonance, the occurrence of triads for a sheared fluid with three-dimensional effects has been demonstrated [22]. For a two-layer fluid with linear current in one or both layers and a wavy seabed, triads and weakly nonlinear evolution equations have been given too [23].

Remarks on the theoretical studies of coupled triads in the context of general physics are in order. If two pairs of triads share *two* members in common, i.e., only four distinct waves are present, significant theoretical advances can be achieved. As examples, there may be Hamiltonian systems with Lax representation [24], and a "solitonic sector of the parameter space" can exist [25]. If the two pairs of triads share only *one* member in common, the role that common member plays in each triad may affect the dynamics dramatically [26–28]. The magnitudes of the difference of the phase angles from these complex-valued wave envelopes will dictate the evolution of the wave profile. A more precise measure of this difference, known as the "dynamical phase," will be defined in the subsequent analysis (Sec. VI B) [29]. In the language of dynamical systems, the governing equations can be shown to be "integrable" through consideration of a Hamiltonian [26]. The widely studied nonlinear Schrödinger equation in fluids, optics, and plasma possesses peculiar properties in a multiwaveguide setting. Coupling produces stronger modulation instability than waveguides alone themselves. We shall show that this statement holds true for coupled triads too.

The goal of the present work is to highlight the existence of new coupled triads for interfacial and internal waves, and in particular, those arising from the presence of stratification or shear current. We focus on triads with participating waves moving in the same directions. For different wave packets to have significant interactions or possibly energy exchanges, their group velocities should not differ widely in magnitude, otherwise the packets will separate before any dramatic nonlinear effects can be observed. In optics, this separation is frequently termed "walk-off effect" [30]. Hence it is desirable to have interacting modes to move in the same direction and similar group velocities if possible. In practice this might not be achieved perfectly, since the wave numbers and frequencies (and hence group velocities) are dictated by the resonance condition.

The sequence of presenting the topics can now be explained. Typical examples with minimal algebraic complexity are discussed (Sec. II and Appendix E). The first example is a single-layer stratified fluid with constant buoyancy frequency confined within a channel with rigid walls. The dispersion relation is a rational function involving quadratic polynomials. The second example is a two-layer, piecewise homogeneous fluid with a free upper surface. A linear shear current is permitted in the upper fluid. The dispersion branches of the surface and interfacial modes moving against the current might approach each other, but never actually intersect. This configuration can readily generate coupled triads with all five modes traveling against the shear flow.

The evolution equations for modulated envelopes are derived by multiple-scale perturbation theory (Sec. III). The usage of amplitude equations is justified for slowly varying approximations.

Numerically, we shall evaluate for simplicity only the interaction coefficients for the continuously stratified fluid case. The relative signs of these interaction coefficients are critical to the dynamical properties [3,6,10,16].

The importance of studying multiple triads is that such coupled triads will lead to either enhanced instability, or new instability which is otherwise absent if each component triad evolves in isolation (Sec. IV). Recently there is intensive interest in the connection between modulation instability and the occurrence of rogue waves. Such new instability due to coupling might be a valuable indicator for the onset of these surprisingly large displacements. The actual derivation of rogue waves for isolated triads has been given in the literature but the significance in fluid dynamics has not been fully examined (Sec. V). We first examine the issues from a theoretical standpoint and contrast the amplification factor with the Peregrine soliton of the nonlinear Schrödinger equation. From a practical standpoint, we use the numerical values of the interaction coefficients of the evolution equations to estimate the amplitude of an "internal rogue wave." Preliminary computations show that such amplitude can be much larger than that of a surface rogue wave.

As a simplified model to scrutinize the general dynamics, we focus on a reduced system by considering only the temporal evolution (Sec. VI). Theoretically, the Madelung representations are utilized, and special parameter regimes are identified where an invariant in addition to the Manley-Rowe relations may exist. The development of the amplitude in time is then approximated by differential equations considerably more complicated than those of elliptic functions for the isolated triad case. Computer simulations are performed to demonstrate the energy-exchange mechanisms and spontaneous generation of signals previously absent from the initial conditions. Finally, conclusions are drawn (Sec. VII).

II. EXAMPLE OF COUPLED TRIADS

We focus on coupled triads where the common member is a "parent" wave ($\boldsymbol{k}_3$, ω_3 below). A parent wave is the one resulting from the interaction of the other two modes, i.e., one with wave number ($\boldsymbol{k}$) and frequency (ω) being sum of the other two modes. Modes 1, 2, 4, 5 will be termed "daughter" waves in this terminology:

$$\boldsymbol{k}_3 = \boldsymbol{k}_1 + \boldsymbol{k}_5, \quad \omega_3 = \omega_1 + \omega_5, \quad \text{and} \quad \boldsymbol{k}_3 = \boldsymbol{k}_2 + \boldsymbol{k}_4, \quad \omega_3 = \omega_2 + \omega_4, \quad \boldsymbol{k}_1 \neq \boldsymbol{k}_2. \tag{1}$$

We must remark that this terminology of naming "parent–sibling–daughter" is not uniform in the literature. Equation (1) represents a theoretical setting for a general wave-number vector $\boldsymbol{k}$. In subsequent discussion, we restrict the attention to the case of horizontal propagation and shall use a scalar wave number k. Examples involving a continuously stratified fluid will be discussed. With the Boussinesq approximation, small-amplitude disturbance is governed by the Taylor-Goldstein equation with vertical velocity (v) and eigenfunction $\phi(z)$ given as (c = phase speed, ε = a (numerically small) amplitude parameter, c.c. = complex conjugate)

$$v = \varepsilon\phi(z)\exp\left[i(kx - \omega t)\right] + \text{c.c.} + O(\varepsilon^2), \tag{2}$$

$$(U - c)\left(\frac{d^2\phi}{dz^2} - k^2\phi\right) - \frac{d^2U}{dz^2}\phi + \frac{N^2\phi}{U - c} = 0. \tag{3}$$

Vertical propagation is excluded due to the presence of rigid walls. N^2 is the square of the buoyancy frequency for a background density profile $\bar{\rho}(z)$:

$$N^2 = -\frac{g}{\bar{\rho}}\frac{d\bar{\rho}(z)}{dz}. \tag{4}$$

In the absence of shear flow [i.e., $U(z) = 0$], the Taylor-Goldstein equation [Eq. (3)] can be simplified considerably for a fluid with constant buoyancy frequency N_0. We exclude wave propagation in the vertical direction by considering a rigid-wall channel of depth H. The dispersion

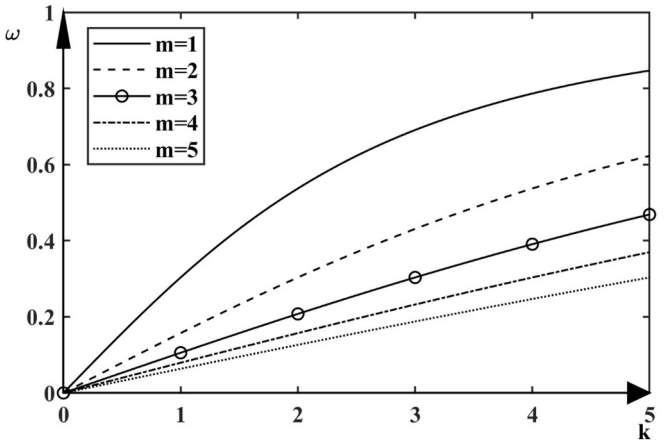

FIG. 1. The dispersion relation, angular frequency ω versus wave number k, for a fluid of constant buoyancy frequency N_0 with m being the mode number ($N_0 = 1, H = 1$).

relation is [10,31] (Fig. 1)

$$\omega^2 = \frac{k^2 N_0^2}{\left(k^2 + \frac{m^2\pi^2}{H^2}\right)}, \quad c = \omega/k. \tag{5}$$

The eigenfunction of Eq. (3) attains a remarkably simple form of

$$\phi(z) = \sin(m\pi z/H), \quad \phi(0) = \phi(H) = 0, \quad m = \text{mode number}. \tag{6}$$

The integer m will be termed the "mode number." Physically it will represent the number of nodes ("$m-1$" point(s) of zero displacement) in the profile of the vertical velocity [Eq. (6)]. Theoretically "m" will define the vertical velocity and eigenfunction profile. The interaction coefficients in the nonlinear analysis will be determined from the solvability condition in a perturbation expansion. As an illustrative example of coupled triads, we consider a set involving modes $m = 1, 3, 5$ and another set involving modes 2, 3, 4 (Figs. 2 and 3), with mode 3 as the common member [Eqs. (1) and (5)]. A graphical search starts with a fixed point on one branch of the dispersion curves. We draw the

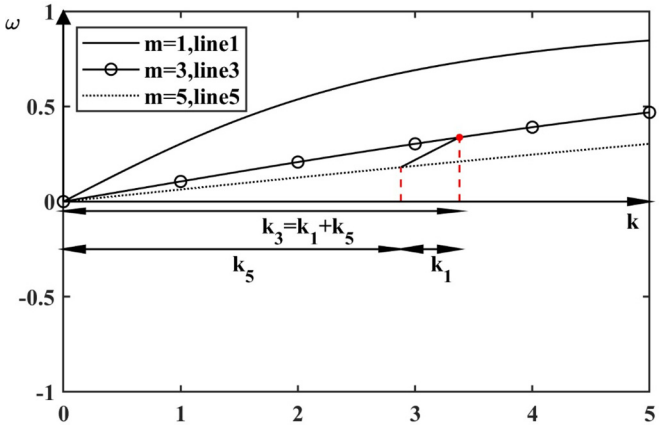

FIG. 2. Graphical construction of a triad.

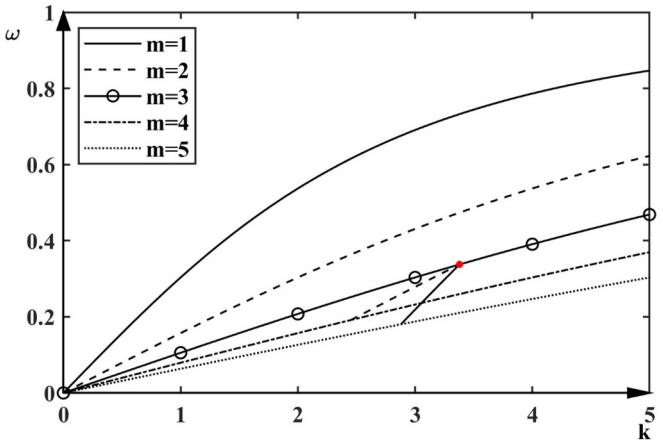

FIG. 3. Schematic diagram of coupled triads [Eqs. (1) and (5)] with all five participating waves traveling in the same direction. A solid dot on the $m = 3$ branch represents the common member, with modes 1, 5, 3 forming one triad and modes 2, 4, 3 the other triad.

various branches of the dispersion curves using this fixed point as the new origin of a Cartesian plane. We then search for intersection points with other branches in the original drawing [1]. The dispersion branches represented by Eq. (5) are convex upwards, with decreasing magnitude with increasing m. In general, intersection of branches according to this graphical construction scheme for various values of m can be found (Figs. 2 and 3). Analytically, we can also confirm the existence of resonance for, say, a "$k_3 = k_1 + k_5$" triad by solving the equation

$$(k_1 + k_5)/[(k_1 + k_5)^2 + 9\pi^2/H^2]^{1/2} = k_1/\left[k_1^2 + \pi^2/H^2\right]^{1/2} + k_5/\left[k_5^2 + 25\pi^2/H^2\right]^{1/2} \qquad (7)$$

for input parameters of k_1, k_5. Typically there are two roots for k_5 for a given k_1. We shall choose the numerically smaller root for discussion (Fig. 4), as large values of wave numbers will not work well for asymptotic scaling for subsequent analysis of slowly varying wave packets.

Given a fixed depth of oceanic waveguide, there are many families of internal modes defined through the vertical velocity eigenfunction of the Taylor-Goldstein equation. These modes from the various families may satisfy the triad resonance condition, i.e., sum of frequencies and wave

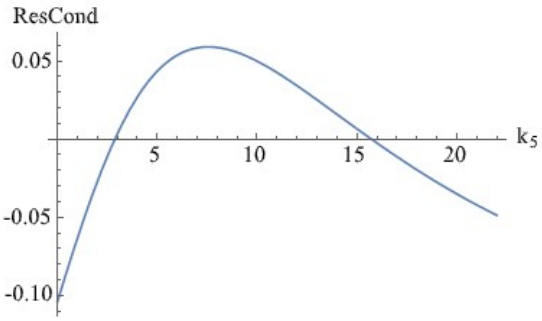

FIG. 4. Computations of the triad resonance condition, Eq. (7), for typical input parameters ($k_1 = 0.5$) showing the existence of two possible values for k_5. We adopt the smaller roots ($k_5 = 2.8787$) in subsequent calculations.

TABLE I. Representative numerical examples of coupled triad resonances in a uniformly stratified fluid.

Grouping of the triads	Wave number k	Angular frequency ω	Mode number of the internal wave m
First set: $k_3 = k_1 + k_5$ $\omega_3 = \omega_1 + \omega_5$	$k_1 = 0.5000$	$\omega_1 = 0.1572$	$m = 1$
	$k_3 = 3.3787$	$\omega_3 = 0.3375$	$m = 3$
	$k_5 = 2.8787$	$\omega_5 = 0.1803$	$m = 5$
Second set: $k_3 = k_2 + k_4$ $\omega_3 = \omega_2 + \omega_4$	$k_2 = 0.9277$	$\omega_2 = 0.1461$	$m = 2$
	$k_3 = 3.3787$	$\omega_3 = 0.3375$	$m = 3$
	$k_4 = 2.4510$	$\omega_4 = 0.1914$	$m = 4$

numbers of two modes being equal to those of the third member. More precisely, we give some concrete examples for the numerical values for the participating modes in Table I [m refers to the mode number, Eqs. (5) and (6)]:

The angular frequency ω being positive (negative) refers to a wave moving to the right (left), respectively. Mode 3 ($m = 3$) is now the common member of the two triads.

A remark on the choice of buoyancy frequency profile is in order. Obviously, the situation of constant N is analytically the simplest one and is frequently used in the literature too [9–12]. The case of a sharply peaked frequency profile

$$N^2 = g\beta_2 \mathrm{sech}^2(\beta_1 z), \quad \beta_1, \beta_2 = \text{real, positive parameters} \tag{8}$$

will permit analytical solutions of the Taylor-Goldstein equation in terms of hyperbolic secant and tangent functions [6]. From the viewpoint of applications, Eq. (8) provides a plausible model in oceanography, as the buoyancy frequency can be large in the thermocline but weak in the abyss [9]. Such studies will constitute the future extension of the present work. Another example of coupled triads will be a two-layer fluid with a shear current [32–35]. This will be further discussed in Sec. VII and Appendix E.

A note on the instability of nonlinear dynamical systems might be useful. For the widely studied nonlinear Schrödinger equation applicable to fluid mechanics and optics, modulation instability refers to the growth of small-amplitude disturbances imposed on a plane or continuous wave (or Stokes wave in the hydrodynamic surface wave context). This instability arises from the interplay of dispersive and nonlinear effects. Obviously, growth of linear disturbances cannot sustain forever and typically periodic motions like the intensively studied Fermi-Pasta-Ulam-Tsingou recurrence (FPUT) [36] may occur.

For three-wave interactions, instability may refer to the spontaneous generation of one wave component of a triad when only two of this resonance group are present initially. For the case where two members of the triad have wave number and frequency half of those of the third member, this scenario is described as subharmonic resonance [1,9]. For optics, a member strong in intensity and capable of producing other members of the triad through resonant interaction is termed the "pump beam."

Amplitudes of the wave components of triads will typically satisfy constraints or conservation laws of the Manley-Rowe relations [1]. When amplitude of one member grows, the energy of the other components will decrease correspondingly, unless these waves belong to the "explosive triads" category. These issues have been discussed in the literature [1,9]. However, one aspect perhaps still deserves studies in the future, i.e., the dynamics of breather/pulsating modes and recurrence phenomena of the FPUT type.

III. NONLINEAR EVOLUTION OF THE TRIAD RESONANCE

To study the dynamics further, we shall conduct the nonlinear analysis for one of the previous examples, namely the continuously stratified case. The procedure of multiple-scale perturbation theory applied to slowly varying wave trains is standard [2,27], and the explanation will be brief.

The second-order perturbation expansion for the horizontal velocity would be

$$u = \varepsilon \sum_m u_1^{(m)} \exp(i\Theta_m) + \varepsilon^2 \sum_m u_2^{(m)} \exp(i\Theta_m), \quad \Theta_m = k_m x - \omega_m t, \quad m = 1, 2, 3, 4, 5, \tag{9}$$

where the summation extends over all five relevant modes, ε is the small-amplitude parameter, and *only* relevant terms in the derivation are kept at $O(\varepsilon^2)$. The induced mean flow will only be needed in the derivation of a nonlinear Schrödinger equation. Similar expansion schemes apply to the vertical velocity, density, and pressure.

The first-order or linear approximation for the fluid dynamics quantities of velocities and density are (Φ_m satisfying the Taylor-Goldstein equation [Eq. (3)]):

$$v_1^{(m)} = B_m \Phi_m(z), \quad u_1^{(m)} = \frac{iB_m}{k_m} \frac{d(\Phi_m(z))}{dz}, \quad \rho_1^{(m)} = i \frac{d\bar{\rho}(z)}{dz} \frac{B_m \Phi_m(z)}{k_m (U - c_m)}, \quad B_m = B_m(\hat{x}, \tau), \tag{10}$$

where B_m is the slowly varying amplitude expressed in slow scales of space and time,

$$\hat{x} = \varepsilon x, \quad \tau = \varepsilon t. \tag{11}$$

In working out the second-order [$O(\varepsilon^2)$] terms in the perturbation expansion for each mode, there will be additional contributions in the inhomogeneous side of the differential equations owing to the triad resonance condition [Eq. (1)], which effectively means that

$$\Theta_3 = \Theta_1 + \Theta_5, \quad \Theta_3 = \Theta_2 + \Theta_4. \tag{12}$$

These inhomogeneous terms must satisfy the solvability conditions as required by the Fredholm alternative theorem, i.e., they must be orthogonal to the null space of the adjoint operator (or the Taylor-Goldstein equation in this case). This constraint will now yield the evolution equations in the slow timescale τ:

(1) First pair of triad:

$$\frac{\partial B_1}{\partial \tau} + c_{g1} \frac{\partial B_1}{\partial \hat{x}} = r_1 B_3 B_5^*; \quad \frac{\partial B_5}{\partial \tau} + c_{g5} \frac{\partial B_5}{\partial \hat{x}} = r_5 B_3 B_1^*; \tag{13a}$$

(2) Second pair of triad:

$$\frac{\partial B_2}{\partial \tau} + c_{g2} \frac{\partial B_2}{\partial \hat{x}} = r_2 B_3 B_4^*; \quad \frac{\partial B_4}{\partial \tau} + c_{g4} \frac{\partial B_4}{\partial \hat{x}} = r_4 B_3 B_2^*; \tag{13b}$$

(3) Common member:

$$\frac{\partial B_3}{\partial \tau} + c_{g3} \frac{\partial B_3}{\partial \hat{x}} = r_{3a} B_1 B_5 + r_{3b} B_2 B_4, \tag{13c}$$

where c_{gm} is the group velocity of the m th mode, $m = 1, 2, 3, 4, 5$. The interaction coefficients "r" are computed by rather lengthy formulations described in Appendix A. The values of wave numbers (k_1 to k_5) involved in the figures below range from 0.5 to 8.0, with larger numbers associated with the higher-order modes like $m = 3, 4, 5$. The values of angular frequencies (ω_1 to ω_5) range from 0.15 to 0.65.

It will be instructive to investigate the dependence of these interaction coefficients on the fluid dynamics input parameters, namely the channel depth and buoyancy frequency. For the purpose of comparison, the common member of the coupled triads is fixed, but the wave numbers of other participating members may vary. In general, the coefficients may change substantially with the depth H, but the variations tend to level off for the limits of small and large values of H (Fig. 5).

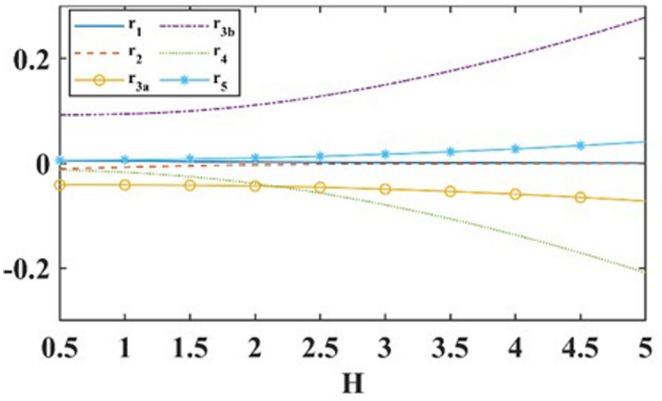

FIG. 5. Variation of the interaction coefficients with the channel depth H.

On the other hand, the variation of the interaction coefficients "r" [Eq. (13)] with the buoyancy frequency can be given analytically. Indeed, it is remarkable that this dependence is completely linear, as illustrated in Fig. 6. This has been verified both numerically and theoretically, with details given in Appendix B. With the increase in buoyancy frequency, oscillations will be enhanced in general. Hence, wave interaction phenomena would take place more rapidly too.

IV. NEW MODULATION INSTABILITY DUE TO COUPLING

A. Overview and formulation

For an isolated, single triad involving three modes, two modes can generate the initially absent third mode of the triad [1,2,9]. This process will still be loosely termed "instability" in the literature, even though the "energy" (as measured by the Manley-Rowe relations) of the three-wave system is conserved. Terms like parametric instability and subharmonic instability (for the special case where the two daughter modes have frequency and wave number half of those of the parent) have also been used. A special case is a plane wave for one mode, while the other two modes of the triad are numerically small in amplitude. Disturbances (or "modulations") on the plane-wave train may generate instability and growth of the other two modes. Following the terminology of the

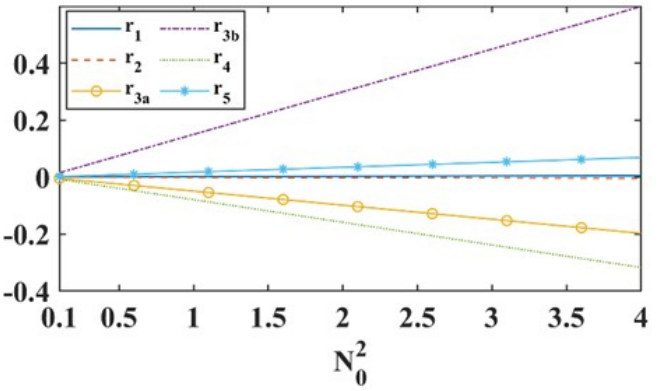

FIG. 6. Direct proportional relation between the interaction coefficients r and the buoyancy frequency N for various fluid scenarios. For each value of N, the configuration under investigation is a stratified fluid with constant buoyancy frequency $N = N_0$.

widely studied nonlinear Schrödinger equation and wave packets in fluids and optics, we term this growth phase a "modulation instability" of a triad. The features of coupling are the occurrence of additional bands of instability and the enhancement of instability rates, even if an isolated triad displays instability.

Self-interaction and the narrow-band assumption of the four-wave interaction process lead to the nonlinear Schrödinger equation, and a comparison with the present situation is instructive. Coupled nonlinear Schrödinger equations can give rise to new instability, and this result was established in a general physical setting in the 1980s [37]. In the context of hydrodynamic waves, two wave trains propagating obliquely to each other have been used to model "crossing sea states" [38]. These scenarios are important in ocean engineering, as field data indicate that such sea states are frequently present for many maritime disasters and accidents. Our goal is to demonstrate this enhanced instability due to coupling occurs for coupled triads in the dynamics of internal waves too. The calculations using realistic values of wave numbers and interaction coefficients will be involved and lengthy formulas will be reported in Appendix C.

Starting with Eqs. (13a)–(13c), we first establish the plane-wave configurations theoretically as

$$\begin{aligned} B_j &= \rho_j \exp[i(\xi_j \hat{x} - \zeta_j \tau)], \quad j = 1, 2, 4, 5 \\ B_3 &= i\rho_3 \exp[i(\xi_3 \hat{x} - \zeta_3 \tau)], \end{aligned} \tag{14}$$

with $\rho_n, \xi_n, \zeta_n, n = 1, \ldots 5$, being the amplitude, wave number, and angular frequency of the plane waves, respectively. The dispersion relation is

$$\begin{aligned} \zeta_j &= c_{gj}\xi_j - r_j \frac{\rho_3 \rho_l}{\rho_j} \quad [\text{for triad pairs } (j, l)] \\ \zeta_3 &= c_{g3}\xi_3 + r_{3a}\frac{\rho_1 \rho_5}{\rho_3} + r_{3b}\frac{\rho_2 \rho_4}{\rho_3}. \end{aligned} \tag{15}$$

In accordance with the standard procedure on studying modulation instability, we now introduce small disturbance:

$$\begin{aligned} B_j &= \rho_j(1 + \rho_j') \exp[i(\xi_j \hat{x} - \zeta_j \tau)], \quad j = 1, 2, 4, 5 \\ B_3 &= i\rho_3(1 + \rho_3') \exp[i(\xi_3 \hat{x} - \zeta_3 \tau)]. \end{aligned} \tag{16}$$

The primes denote small disturbances. Substituting Eq. (16) into Eq. (13) and linearization yield stability formulation of five algebraic equations (Appendix C). To obtain the criterion of instability, one further assumes

$$\rho_j' = P_j + iQ_j \quad (\rho_j')^* = P_j - iQ_j \quad j = 1, .., 5, \tag{17}$$

and looks for normal modes through

$$P_j = p_j \exp[i(K\hat{x} - \Omega\tau)], \quad Q_j = q_j \exp[i(K\hat{x} - \Omega\tau)], \quad j = 1, .., 5. \tag{18}$$

For instability to occur, the 10 algebraic equations must admit nontrivial solutions for p_j, q_j. The resulting 10×10 determinant will give the criterion of instability. For comparison, the corresponding matrices for an isolated triad involving modes (1, 5, 3) and modes (2, 4, 3) are also given (Appendix C).

B. Coupling-induced and coupling-enhanced instabilities

The terms "baseband" ("passband") instability will be adopted, corresponding to long (finite) wavelength instability respectively, with the former associated with the occurrence of rogue waves [34].

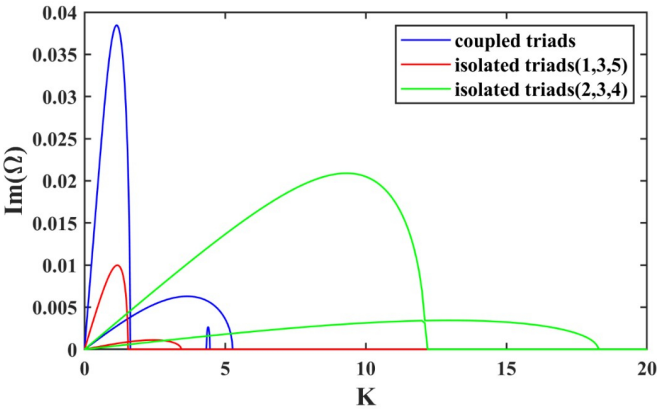

FIG. 7. Both the (1, 5, 3) and (2, 4, 3) triads are unstable by themselves, but coupling produces an even stronger instability.

1. First example

We first demonstrate that coupled triads can lead to enhanced instabilities compared with those displayed by isolated triads. For the purpose of illustration we adopt the modes with wave numbers indicated in earlier sections where the interaction coefficients are given by

$$
\begin{aligned}
&r_1 = 4.189(10^{-3}), \quad r_2 = -7.618(10^{-3}), \quad r_{3a} = -4.144(10^{-2}),\\
&r_{3b} = 9.410(10^{-2}), \quad r_4 = -1.719(10^{-2}), \quad r_5 = 6.315(10^{-3}),\\
&c_{g1} = 3.066(10^{-1}), \quad c_{g2} = 1.541(10^{-1}), \quad c_{g3} = 8.850(10^{-2}),\\
&c_{g4} = 7.524(10^{-2}), \quad c_{g5} = 6.058(10^{-2}).
\end{aligned}
$$

Both triads exhibit instability by themselves. However, a coupled state will produce a stronger instability (Fig. 7). The amplitudes of the plane waves are given by $\rho_1 = \rho_2 = \rho_3 = \rho_4 = \rho_5 = 10$.

2. Second example

The interaction coefficients in the previous example are small in absolute magnitude, and are thus inconvenient in illustrating a coupling-induced instability. Hence we adopt these parameter values to illustrate the existence of new instability (Fig. 8):

$$
\begin{aligned}
&c_{g1} = 0.5, \quad c_{g5} = 1, \quad c_{g3} = 0, \quad c_{g2} = 1, \quad c_{g4} = 2,\\
&r_1 = 1, \quad r_5 = -1, \quad r_2 = 1, \quad r_4 = -1, \quad r_{3a} = 1, \quad r_{3b} = 1,\\
&\rho_1 = 2, \quad \rho_5 = 1, \quad \rho_2 = 2, \quad \rho_4 = 1, \quad \rho_3 = 0.5,\\
&\xi_1 = -12.5, \quad \xi_5 = 13.5, \quad \xi_2 = -5.25, \quad \xi_4 = 6.25, \quad \xi_3 = 1,\\
&\zeta_1 = -6.5, \quad \zeta_5 = 14.5, \quad \zeta_2 = -5.5, \quad \zeta_4 = 13.5, \quad \zeta_3 = 8,
\end{aligned}
$$

and for comparison, the configuration and input parameters for the uncoupled cases are

$$
\begin{aligned}
&r_1 = 1, \quad r_5 = -1, \quad r_{3a} = 1, \quad \rho_1 = 2(2)^{1/2} = 2.828, \quad \rho_5 = (2)^{1/2} = 1.141, \quad \rho_3 = 0.5,\\
&r_2 = 1, \quad r_4 = -1, \quad r_{3b} = 1, \quad \rho_2 = 2(2)^{1/2} = 2.828, \quad \rho_4 = (2)^{1/2} = 1.141, \quad \rho_3 = 0.5.
\end{aligned}
$$

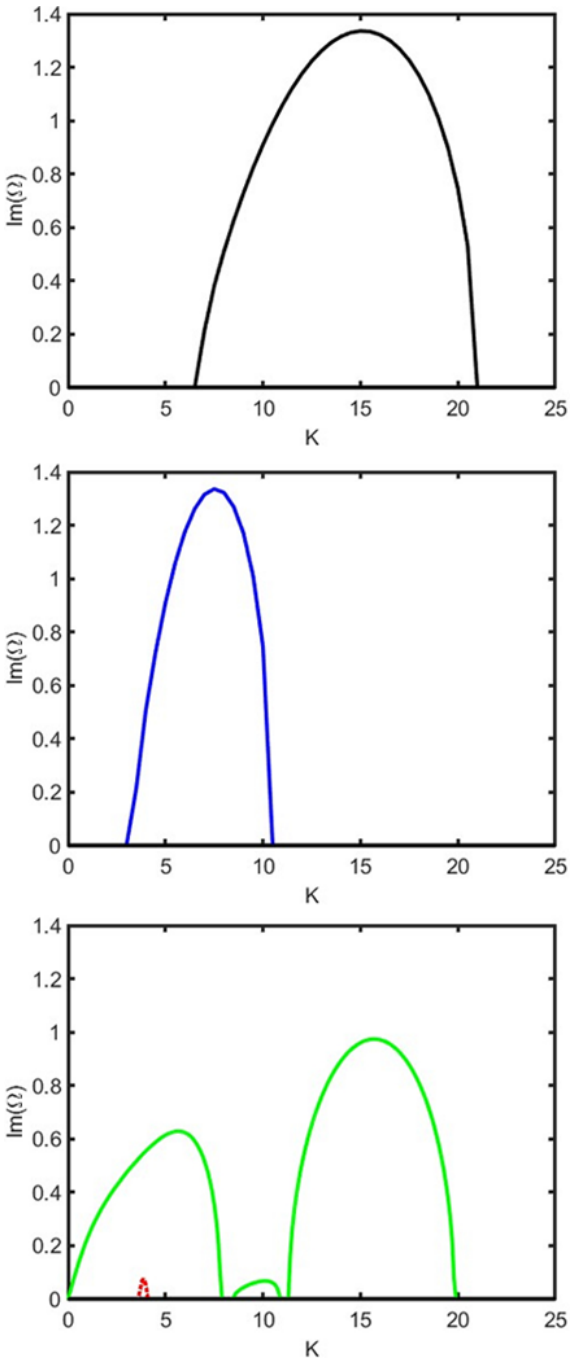

FIG. 8. Triads on their own exhibit passband instability only. Top: isolated (1, 3, 5) triad; Middle: isolated (2, 3, 4) triad. Bottom: Coupling induces baseband (small wave number) instability (solid curve) and additional passband instability (dotted curve).

We loosely name an instability branch as a "baseband" branch as long as that curve indicates instability in the long wave-number regime. That region is the critical portion in association with the existence of rogue waves.

V. ROGUE MODES FOR INTERNAL WAVES

A. Motivation and background

While rogue waves as unexpectedly large displacements have been studied intensively for surface waves, similar inquiries on internal modes in the oceans have not been fully examined. The few existing works focus on the long wave regimes, using the Gardner equation as a model, which basically is a Korteweg–de Vries equation with both quadratic and cubic nonlinearities [39–41]. We propose that studying "rogue internal waves" in the finite-wavelength regime using the triad equations will provide a fruitful direction of research. It will be instructive to contrast with studies of rogue events for surface waves using the well-established nonlinear Schrödinger equation [42].

B. Theoretical consideration

Unlike the more widely known Peregrine soliton of the nonlinear Schrödinger equation, rogue waves for the three-wave interaction process have only been derived recently [43] and the fluid dynamics implications have not been fully examined. The Peregrine soliton has a maximum amplitude of three times the background plane wave [27]. The higher-order rogue waves of the nonlinear Schrödinger equation have maximum displacements being an odd integer multiple of the background, i.e., amplification factors of five and seven for the second and third-order rogue waves. The second-order rogue wave has been experimentally realized in a laboratory [44].

In contrast, the rogue waves for even an isolated triad in a normalized form, i.e.,

$$\begin{aligned}
&\partial\Psi_1/\partial\tau + V_1\partial\Psi_1/\partial\hat{x} = \Psi_2\Psi_3{}^*, \quad \partial\Psi_2/\partial\tau + V_2\partial\Psi_2/\partial\hat{x} = -\Psi_1\Psi_3,\\
&\partial\Psi_3/\partial\tau + V_3\partial\Psi_3/\partial\hat{x} = \Psi_2\Psi_1{}^*,
\end{aligned} \tag{19}$$

display a much higher degree of algebraic complexity. More precisely, their forms are [43]

$$\begin{aligned}
\Psi_1 &= 2q\delta_1\left[1 + \frac{3\sqrt{3}u_0^*\theta^* u_1}{|u_0|^2 + |u_1|^2 + |u_2|^2}\right]\exp[i(K_1\hat{x} + q\tau)],\\
\Psi_2 &= 2q\delta_2\left[1 + \frac{3\sqrt{3}u_0^*\theta u_2}{|u_0|^2 + |u_1|^2 + |u_2|^2}\right]\exp[i(K_2\hat{x} - q\tau)],\\
\Psi_3 &= 2iq\delta_3\left[1 + \frac{3\sqrt{3}u_1^*\theta^* u_2}{|u_0|^2 + |u_1|^2 + |u_2|^2}\right]\exp[i(K_2 - K_1)\hat{x} - 2iq\tau].
\end{aligned} \tag{20}$$

The auxiliary expressions are

$$\begin{aligned}
&u_0 = \gamma_1 + \gamma_2\varsigma_1 + \gamma_3(\eta - i\theta^*), \quad u_1 = \gamma_1 + \gamma_2(\varsigma_1 + \theta^*) + \gamma_3\left(\eta + \theta^*\varsigma_1 + i\sqrt{3}\right),\\
&u_2 = \gamma_1 + \gamma_2(\varsigma_1 + \theta) + \gamma_3(\eta + \theta\varsigma_1), \quad \varsigma_1 = -2q(\tau + i\rho_1\hat{x}), \quad \eta = \left(\varsigma_1^2\right)/2 - 2iq\rho_2\hat{x},\\
&\rho_1 = \theta/V_1 - \theta^*/V_2, \quad \rho_2 = 1/V_1 - 1/V_2,\\
&K_1 = q\left(\frac{1}{V_1} - \frac{2}{V_2}\right), \quad K_2 = q\left(\frac{2}{V_1} - \frac{1}{V_2}\right),\\
&\theta = (-\sqrt{3} + i)/2,\\
&\delta_1 = \sqrt{1 - \frac{V_2}{V_1}}, \quad \delta_2 = \sqrt{\frac{V_1}{V_2} - 1}, \quad \delta_3 = \frac{V_1 - V_2}{\sqrt{V_1V_2}} = \delta_1\delta_2,
\end{aligned}$$

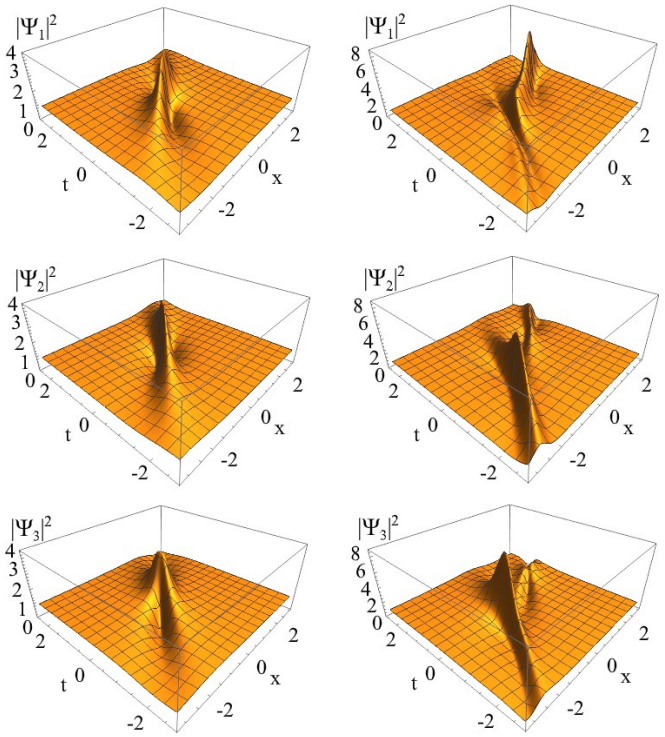

FIG. 9. Rogue waves for the three components an isolated triad (intensities $|\Psi_n|^2$, $n = 1, 2, 3$ vs space and time). Left column: Profile with one peak ($\gamma_3 = 0$). Right column: Profile with two peaks ($\gamma_3 = 1$); $\gamma_1 = \gamma_2 = q = 1, V_1 = 2, V_2 = 1$.

where the group velocities need to satisfy a constraint $V_1 > V_2 > V_3$. On moving in a frame with velocity V_3, we can set $V_3 = 0$. There are four free parameters, namely, γ_1, γ_2, γ_3, and q. V_1, V_2 are actually not free parameters as they are dictated by the choice of resonant modes. The most important input is γ_3, as γ_3 being zero (nonzero) will imply a quadratic (fourth-order) polynomial in the denominator of Eq. (20) and a wave profile of one (two) peak(s), respectively. A full analysis on the maximum displacement for various γ_n will be left for a future work. Generally speaking, the amplification factor is 2 for $\gamma_3 = 0$, but will be in the range of 2.0 to 3.0 for $\gamma_3 \neq 0$ (Fig. 9). The intensity of the energy, typically proportional to the square of the amplitude, will be four times the background for $\gamma_3 = 0$.

C. Practical consideration

While the theoretical consideration might be a topic of interest to nonlinear science, a practical question might be "how large can an internal rogue wave be?." To address this issue, a crude comparison with surface rogue waves modeled by the nonlinear Schrödinger theory would be an instructive exercise. Extensive field and computational studies have produced "hindcast" studies of rogue waves measured at the oil platforms in the North Sea in Europe. One famous example of such oceanic rogue waves is the Draupner Wave with an amplitude as high as 25 m [45].

If we make the assumption that the Draupner Wave can be modeled by the Peregrine soliton of a nonlinear Schrödinger model, this 25-m amplitude is at least plausible because a rogue wave with three times a background plane wave of say about 8 m will achieve this height. A rough calculation of the coefficients of the nonlinear Schrödinger equation with the water depth conditions relevant to the Draupner case reveals numbers with magnitude unity, and hence no rescaling is

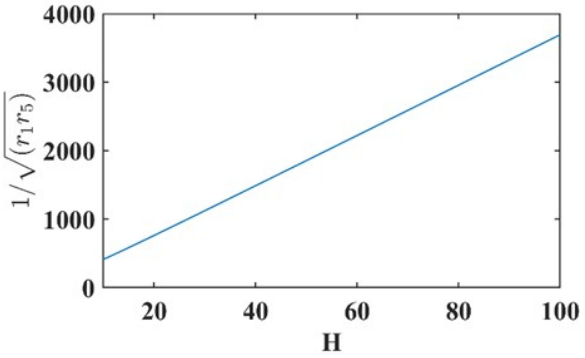

FIG. 10. Scaling factor for converting the dimensional triad system [Eq. (13)] to a nondimensional one like Eq. (19), implying that the magnitude of an internal rogue wave can attain big amplitude due to the large scaling factor.

necessary. We also recognize that there are intense debates on the applicability of the Schrödinger theory as opposed to other mechanisms, e.g., quadratic interactions of waves [46]. Such debates actually highlight the merit of the present approach using resonant interactions, as the evolution equations under consideration actually display quadratic nonlinearities. However, we shall defer detailed investigations of these issues to the future.

Hence we shall just compute an order of magnitude of such an internal rogue wave due to triad resonance. To go from actual fluid dynamics setting of Eqs. (13a) and (13c) to a theoretical description of Eq. (19), one must rescale by

$$B_1 = \Psi_1/(|r_{3a}|r_5)^{1/2}, \quad B_3 = \Psi_2/(r_1 r_5)^{1/2}, \quad B_5 = \Psi_3/(r_1|r_{3a}|)^{1/2}.$$

Hence even though the "normalized" Ψ_n might attain an amplification of two times the background, the interaction coefficients must also be accounted for. Taking typical values from Sec. III, we take as illustrative example the potential magnification ratio for the common member of the triads B_3, i.e., $1/(r_1 r_5)^{1/2}$ (Fig. 10). This amplification ratio can attain values of a few hundreds as the depth takes up values typical of a realistic ocean. Hence displacements due to such internal rogue waves can potentially be tremendous.

VI. DYNAMICS AND SIMULATIONS OF A SIMPLIFIED MODEL

A. Overview

To describe the full dynamics of this system of interacting waves, a full simulation of Eqs. (13a)–(13c) is probably required. Nevertheless, we still hope to capture the main nonlinear physics of energy transfer between triads by ignoring the spatial dependence or the group velocity component, thus effectively looking at the intriguing behavior of the system at a reduced "manifold" [21]. In other words, we focus on the time dependence first. A similar approach has also been adopted in the studies of stratified flows where the buoyancy frequency takes the form of the square of a hyperbolic secant [6]. Alternatively, we interpret this approximation as searching for a pattern depending on time only or working in a configuration where the spatial dependence is periodic or varying on an even slower scale asymptotically.

We shall first perform a theoretical analysis, deriving a few counterparts of the Manley-Rowe type conservation laws for a single triad [1]. The general coupled triad case probably is not "integrable" theoretically. Nevertheless, there are special parameter regimes where an additional invariant, resembling a "Hamiltonian" of the equations of motion, *may* exist. The evolution of

the amplitudes is then approximated by differential equations considerably more complex than the isolated triad case, and cannot be solved by elliptic functions.

A remark on the comparison and contrast with previous theoretical works on coupled triads is in order. Investigations on the coupled triad equations have been conducted in the literature, where the common member can either be a parent or a daughter wave [26,27], as explained in Sec. II. The emphasis is usually on the case of interaction coefficients being all unity (or in a 1:2 ratio). As the results of Sec. III show, these interaction coefficients vary widely in magnitude and cannot in general be scaled all to unity. Numerical simulations for the case where the common member was the daughter wave [k_1, k_2, k_4, k_5 of Eq. (1)] had been performed [24,25]. Here the analysis is conducted for the case where the common member is the parent wave [k_3 of Eq. (1)]. The role of the relative difference in phase angles of the complex wave envelopes again proves to be significant.

These simulations also elucidate the transfer of energy among triads, in particular highlighting how modes absent initially can be excited by others. This spontaneous generation is especially striking as modes grow due to members from the other triad, the common member serving as the catalyst in the energy transfer.

B. Analytical formulation

Following the notations earlier in the literature [1], we first normalize the amplitudes such that most of the interaction coefficients have magnitude unity. This can be achieved by implementing "$B_m = (\text{scaling constant})\, A_m$" in Eq. (13), $m = 1, 2, 3, 4, 5$, i.e., we study

$$\begin{aligned}
&\frac{dA_1}{d\tau} = s_1 A_3 A_5^*, \quad \frac{dA_5}{d\tau} = s_5 A_3 A_1^*, \quad s_1^2 = s_5^2 = 1,\\
&\frac{dA_2}{d\tau} = s_2 A_3 A_4^*, \quad \frac{dA_4}{d\tau} = s_4 A_3 A_2^*, \quad s_2^2 = s_4^2 = 1,\\
&\frac{dA_3}{d\tau} = s_{3a} A_1 A_5 + s_{3b} A_2 A_4.
\end{aligned} \tag{21}$$

In general, only five out of the six interaction coefficients ("s_n") can be scaled to ± 1. For convenience we leave s_{3b} as an arbitrary parameter, and study how the evolution of wave profiles can be affected by varying the values of s_{3b} in Sec. VI C.

If only one set of triad is present, say $A_2 = A_4 = 0$, explosive growth may occur if all the interaction coefficients "s" are of the same sign. Conversely, periodic and localized solutions are possible if one coefficient has a sign different from the other two [1].

To understand the analytical structures and also to formulate a system convenient for the purpose of numerical simulations, we adopt the Madelung representations

$$A_m = b_m \exp(i\eta_m), \quad m = 1, 2, 3, 4, 5, \quad \theta_1 = \eta_1 + \eta_5 - \eta_3, \quad \theta_2 = \eta_2 + \eta_4 - \eta_3. \tag{22}$$

The quantities θ_1, θ_2 will be termed *dynamical phase factors* or simply "dynamical phase." Straightforward calculations now give

$$\frac{db_1}{d\tau} = s_1 b_3 b_5 \cos\theta_1, \quad \frac{db_5}{d\tau} = s_5 b_1 b_3 \cos\theta_1, \quad \frac{db_2}{d\tau} = s_2 b_3 b_4 \cos\theta_2, \quad \frac{db_4}{d\tau} = s_4 b_3 b_2 \cos\theta_2, \tag{23a}$$

$$\frac{db_3}{d\tau} = s_{3a} b_1 b_5 \cos\theta_1 + s_{3b} b_2 b_4 \cos\theta_2, \tag{23b}$$

$$\frac{d\theta_1}{d\tau} = -\left[\frac{s_1 b_3 b_5}{b_1} + \frac{s_5 b_3 b_1}{b_5} + \frac{s_{3a} b_1 b_5}{b_3}\right]\sin\theta_1 - \frac{s_{3b} b_2 b_4}{b_3}\sin\theta_2, \tag{23c}$$

$$\frac{d\theta_2}{d\tau} = -\left[\frac{s_2 b_3 b_4}{b_2} + \frac{s_4 b_2 b_3}{b_4} + \frac{s_{3b} b_2 b_4}{b_3}\right]\sin\theta_2 - \frac{s_{3a} b_1 b_5}{b_3}\sin\theta_1, \tag{23d}$$

and "b_m" can attain negative values in this formulation. Simple manipulation gives

$$s_1 b_1 \frac{db_1}{d\tau} = s_5 b_5 \frac{db_5}{d\tau}, \quad s_2 b_2 \frac{db_2}{d\tau} = s_4 b_4 \frac{db_4}{d\tau}. \tag{23e}$$

Using Eq. (23e), a few Manley-Rowe type "conservation laws" similar to those of isolated triads can be readily derived [1], e.g.,

$$s_1\left[b_1^2 - b_1^2(0)\right] = s_5\left[b_5^2 - b_5^2(0)\right], \quad s_2\left[b_2^2 - b_2^2(0)\right] = s_4\left[b_4^2 - b_4^2(0)\right]. \tag{24}$$

Without further constraint, Eqs. (23a)–(23d) are generally not "integrable." Illustrative numerical simulations from the perspective of mode generation and energy transfer will be discussed in Sec. VI C. Here we highlight possible analytical progress for special cases:

Special case $s_{3a} = s_{3b} = s_3 = \pm 1$

For the conservation law involving the common member, i.e., the k_3, ω_3 mode, we consider only the special case $s_{3a} = s_{3b} = s_3 = \pm 1$. With this assumption, we readily derive

$$s_3\left[b_3^2 - b_3^2(0)\right] = s_1\left[b_1^2 - b_1^2(0)\right] + s_2\left[b_2^2 - b_2^2(0)\right], \tag{25a}$$

or alternatively,

$$s_3\left[b_3^2 - b_3^2(0)\right] = s_5\left[b_5^2 - b_5^2(0)\right] + s_4\left[b_4^2 - b_4^2(0)\right]. \tag{25b}$$

Special case for a possible additional invariant

The quantity

$$\Gamma = b_1 b_3 b_5 \sin\theta_1 + \lambda b_2 b_3 b_4 \sin\theta_2 \tag{26}$$

may become an additional invariant of the dynamics under special circumstances. For an isolated triad with $b_2 = b_4 = 0$, $b_1 b_3 b_5 \sin\theta_1$ is well established as a Hamiltonian. In the present scenario of coupled triads, the time rate of change of Γ [Eq. (26)] will be zero if one of the following holds:

$$\text{(a) } \theta_1 = \theta_2 = 0 \text{ for all } \tau, \tag{27a}$$

$$\text{(b) } d\theta_1/d\tau = d\theta_2/d\tau, \quad \text{or} \quad \theta_2 - \theta_1 = M\pi, \quad M \quad \text{integer}; \tag{27b}$$

$$\text{(c) } s_{3a} = \lambda_{s3b}. \tag{27c}$$

For case (a), $\theta_1 = \theta_2 = 0$ holds for all time and this situation was studied earlier [23]. The governing equations for the amplitudes b_m, $m = 1, 2, 3, 4, 5$, will be associated with cubic polynomials, solvable by elliptic functions in special cases. Case (c) is more involved and will be deferred for future studies.

We shall just treat case (b). We cannot prove analytically that θ_2–θ_1 remains small or tends to zero if this quantity starts off with a small value initially. Similarly, we cannot define the precise initial conditions which will lead to solutions approaching Eq. (27b) for large time. Instead we shall just provide numerical evidence in Sec. VI C to substantiate this conjecture that there are solutions approaching the regime of θ_2–$\theta_1 = M\pi$, M integer. *Assuming* that Eq. (27b) is valid, we can derive an approximate evolution equation for the amplitude which is drastically different from that of the elliptic functions. It is worthwhile to document the intriguing dynamics here.

If the time derivative of Γ [Eq. (26)] is zero, we can in particular choose λ to be $+1$ and -1. Hence further constants of motion can be identified as

$$\Gamma_1 = b_1 b_3 b_5 \sin\theta_1, \quad \Gamma_2 = b_2 b_3 b_4 \sin\theta_2.$$

For simplicity we just consider the case θ_2–θ_1 = even multiple of π. Equations (23c) and (23d) collapse into

$$\frac{s_1 b_5}{b_1} + \frac{s_5 b_1}{b_5} = \frac{s_2 b_4}{b_2} + \frac{s_4 b_2}{b_4}. \tag{28}$$

We now take

$$X(\tau) = s_1\big[b_1^2 - b_1^2(0)\big], \quad Y(\tau) = s_2\big[b_2^2 - b_2^2(0)\big]. \tag{29}$$

The governing equation for $X(\tau)$ is considerably more complicated than the classical elliptic function, and technical details are described in Appendix D.

C. Numerical simulations

While relevant information on the analytical structures of the coupled triads can be extracted from the time invariants and conservation laws, physical insight on the exchange of energy might as well be directly obtained by numerical simulations. For such purpose we go back to Eq. (13) and study how localized pulses in one set of triads can excite displacements in the other set.

From the numerical values obtained in Sec. III and the normalization procedure described at the beginning of Sec. IV, five out of the six interaction coefficients (s_n) can in general be scaled to ± 1. For convenience we leave s_{3b} as an arbitrary parameter. For cases (1) through (3), we shall study Eq. (23) with these interaction coefficients:

$$s_1 = +1, \quad s_2 = -1, \quad s_{3a} = -1, \quad s_{3b} = +1, \quad s_4 = -1, \quad s_5 = +1, \tag{30}$$

except for case (4) (see Fig. 14) and case (5) (see Fig. 15) below. For case (4), we look at the dependence on the parameter s_{3b}, and for case (5) we study other combinations of sign patterns of the interaction coefficients.

In terms of numerical procedure, Eqs. (23a)–(23d) are integrated forward in time using a standard fourth-order Runge-Kutta scheme. Typically, a time step of 0.01 is utilized. Initially ($\tau = 0$) a mode may be absent ($b_n = 0$), present as a small noise ($b_n = 0.0001$), or given a prescribed amplitude ($b_n = 1$). We now describe a few representative scenarios.

(1) The common member of the two coupled triads exciting all the participating modes:

With $b_3(0) = 1$, and $b_n(0) = 0.0001$, $n = 1, 2, 4, 5$, $\theta_1 = \theta_2 = \pi/2$, for the $k_3 = k_1 + k_5$ and $k_3 = k_2 + k_4$ resonance, i.e., only the common member of the two triads is present initially, all modes nevertheless display periodic oscillations subsequently (Fig. 11).

(2) Energy transfer arising from the coupling of triads through the common member:

The initial conditions are now chosen to be

$$b_1(0) = 1, \quad b_5(0) = 1, \quad b_2(0) = b_4(0) = 0.0001, \quad b_3(0) = 0.01, \quad \theta_1 = \theta_2 = \pi/2.$$

In other words, all members of the $k_3 = k_2 + k_4$ triad are negligible initially, including the common member with wave number k_3. At subsequent time, the remarkable features are that the mode A_3 is generated and eventually the A_2, A_4 modes appear too. Energy has thus successfully flowed from one triad to another through a common member (Fig. 12). Further numerical simulations for still larger values in time show that energy flows periodically between the two triads.

Another intriguing feature is the temporal development of the dynamical phase factors, θ_1, θ_2, or more precisely their difference, θ_1–θ_2. While each phase oscillates sinusoidally, the quantity θ_1–θ_2 asymptotically approaches a constant, numerically very close to $-\pi$ (Fig. 12). This dataset provides strong computational evidence that θ_1–θ_2 being an integer multiple of π will constitute special regimes for the nonlinear dynamics.

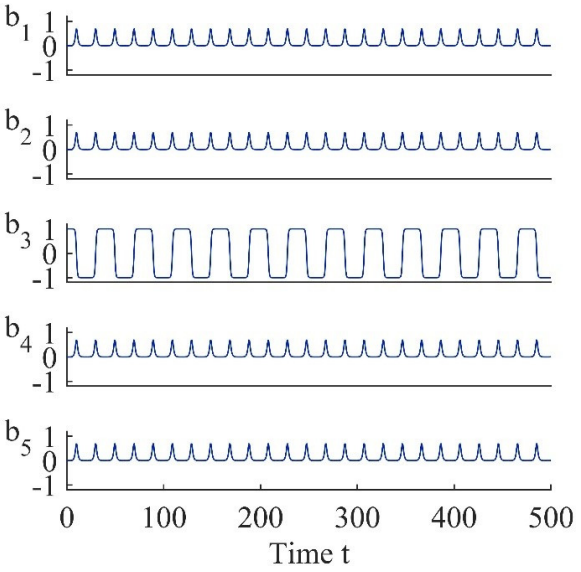

FIG. 11. The common member of the two coupled triads excites all the participating modes. Modes classified as "present (absent)" initially will be given amplitude 1.0/0.0001 at time $\tau = 0$. Only the common member A_3 with wave number k_3 is present initially. The normalized interaction coefficients are given by $s_1 = +1$, $s_2 = -1$, $s_{3a} = -1$, $s_{3b} = +1$, $s_4 = -1$, $s_5 = +1$.

(3) Critical roles of the dynamical phase in the evolution of the wave profile:

The dynamical phase factors θ_1, θ_2 [Eq. (22)] highlight the role of the polar angles of the complex-valued envelopes in the Madelung representations. It has been established that such factors will drastically influence the temporal development of the wave profiles [25,47]. Here we confirm this feature for coupled triad resonance with the parent wave as the common member, by displaying different wave shapes for distinct combinations of dynamical phase factors, namely, $\theta_1 = \pi/2$, $\theta_2 = 0$ versus $\theta_1 = 0$, $\theta_2 = \pi/2$ at $\tau = 0$ (Fig. 13).

(4) Effect of the magnitude of the interaction coefficients:

In general, six interaction coefficients cannot all be scaled to ± 1 in the evolution of five waves. For this purpose, we study the effect of varying s_{3b} while the other five interaction coefficients are taken to have magnitude unity. To illustrate this variation we take values as given by Eq. (26) except for two different scenarios:

(i) $s_{3b} = 3$ [Fig. 14(a)], and

(ii) $s_{3b} = 15$ [Fig. 14(b)].

The wave profiles are clearly different and hence the evolution will critically depend on the magnitude of the interaction coefficients. Energy exchange and excitation of modes will still take place, perhaps just in different forms.

(5) Partial or minimal transfer of energy:

Flow of energy among the triad modes is not automatic and depends critically on the mechanism of coupling, i.e., the values of the interaction coefficients of the dynamical system [Eqs. (21)–(23)]. As an example we consider the combination

$$s_1 = +1, \quad s_2 = -1, \quad s_{3a} = -1, \quad s_{3b} = +1, \quad s_4 = -1, \quad s_5 = -1.$$

Although this combination differs from that of the constant buoyancy frequency case, it is conceivable that such patterns can arise from other stratified flows. For this particular case, energy present initially in the mode A_3 can only be transmitted to A_2 and A_4, while A_1 and A_5 remain effectively at zero amplitude (Fig. 15).

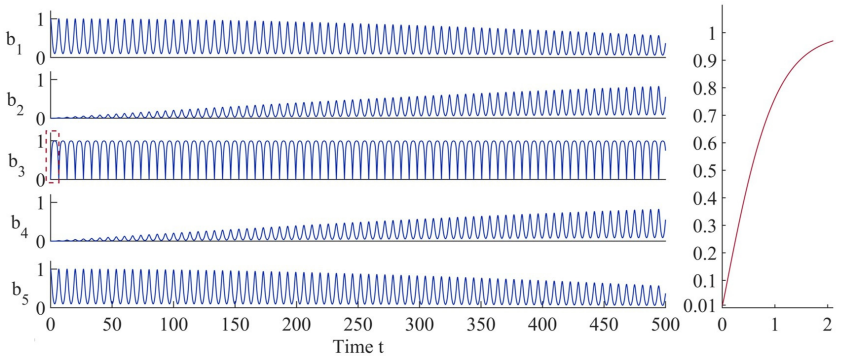

(a)

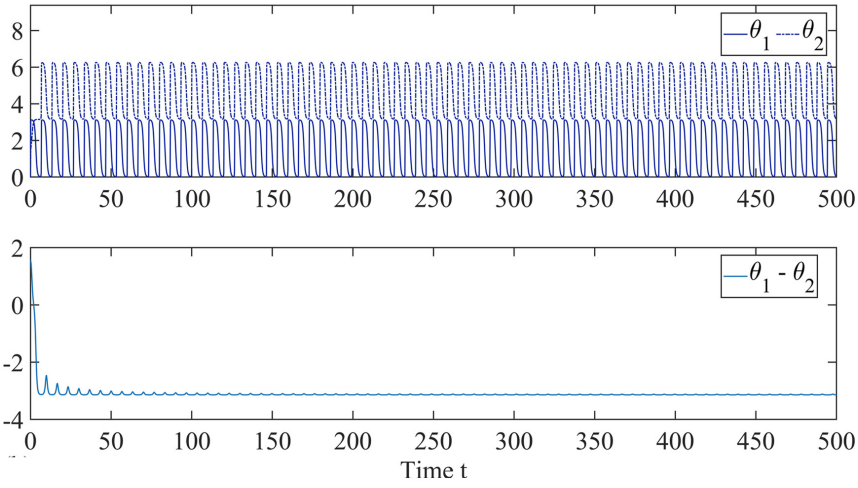

(b)

FIG. 12. (a) Energy transfer arises from the coupling of two triads through the common member. Initially only A_1, A_5 have finite amplitude with $|A_1| = 1$, $|A_2| = 0.0001$, $|A_3| = 0.01$, $|A_4| = 0.0001$, $|A_5| = 1$. A magnified view for b_3 is inserted on the right to show the numerically small (but nonzero) initial condition. Energy flows from the $k_3 = k_1 + k_5$ triad to the $k_3 = k_2 + k_4$ triad through the common member A_3 with wave number k_3. (b) The temporal evolution of the dynamical phase factors θ_1, θ_2: While each phase oscillates sinusoidally, the difference θ_1–θ_2 approaches asymptotically the value of $-\pi$ for large time.

VII. DISCUSSION AND CONCLUSIONS

Coupled triads with all five modes traveling in the same direction are demonstrated to exist for internal waves in a stratified fluid with a constant buoyancy frequency N_0. Qualitatively similar phenomenon can occur for a two-layer fluid with a linear shear, and the details are described in Appendix E. Evolution equations are derived for the first example. The dependence of the interaction coefficients, for various coupled triads with a fixed common member, on the channel height and the buoyancy frequency is elucidated. For simplicity, vertical or oblique propagation of internal waves is excluded.

Coupling may produce enhanced or new instabilities, especially in the long-wavelength regime (known as "baseband instability"). This feature is important as recent works highlight the connection between baseband instability and the possible onset of rogue waves. Analytical solutions for rogue

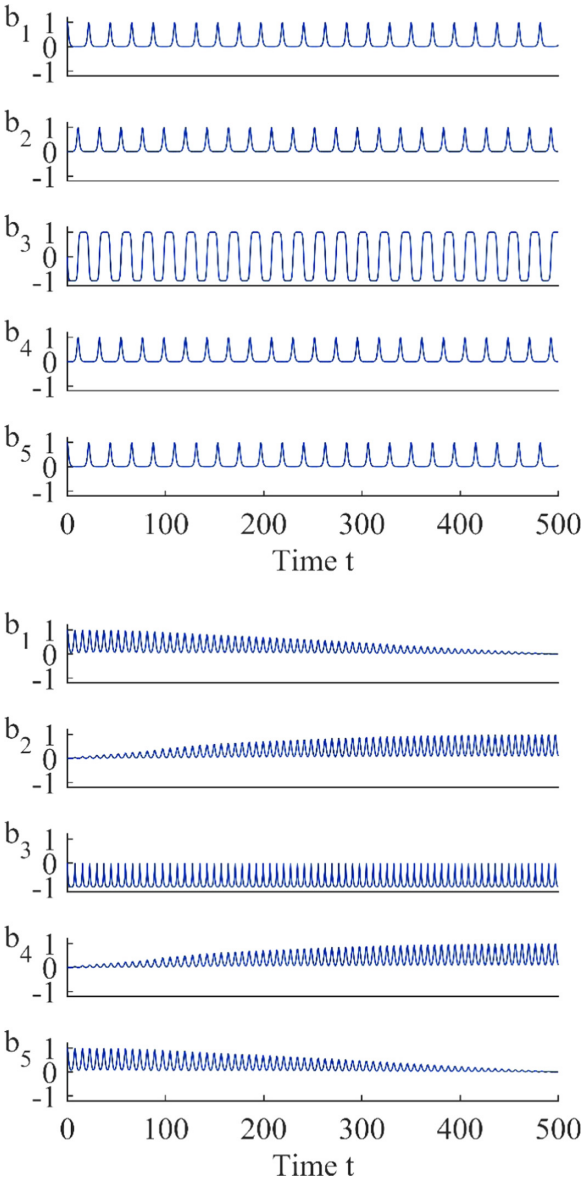

FIG. 13. Effect of the dynamical phase factors [Eq. (22)] in the evolution of the wave profiles. Top: $\theta_1 = 0$, $\theta_2 = \pi/2$; Bottom: $\theta_1 = \pi/2$, $\theta_2 = 0$. Initial conditions are $b_1 = b_5 = 1$, $b_2 = b_4 = 0.0001$, $b_3 = 0.001$.

waves of an isolated triad have been obtained recently in a general physical context. For applications to oceanography, important issues involve the evolution timescale and quadratic nonlinearities, in sharp contrast with the intensively studied cubic nonlinear Schrödinger model for surface rogue waves. Issues like resonance, harmonic generation, and energy transfer among modes are critical in the studies of internal waves [48].

In the theoretical context, by employing the Madelung representations, conservation laws for the wave amplitudes similar to the classical Manley-Rowe relations can be established. While the general evolution equations might not be integrable, there are special parameter regimes for the possible existence of an additional invariant resembling the Hamiltonian of motion. One intriguing

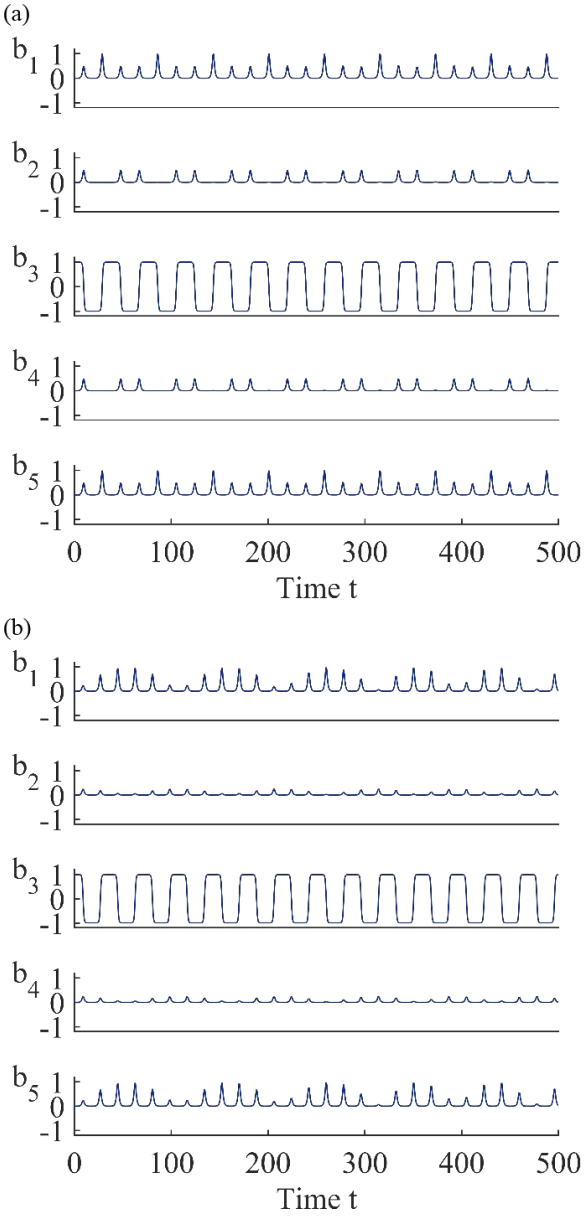

FIG. 14. (a) Effect of varying interaction coefficients; values as given by Eq. (30), except that $s_{3b} = 3$. (b) Same as (a) except that $s_{3b} = 15$.

case arises when the difference of the dynamical phase factors of the two triads differs by an integer multiple of "π." The approximate governing equation for the amplitude then deviates drastically from the one for an elliptic function of an isolated triad. In terms of gaining physical insight directly, numerical simulations demonstrate the spontaneous generation of modes in one triad by wave trains from the other triad. Through these simulations we provide computational evidence that the dynamical phase factors can approach asymptotically to integer multiple of π for large time. Finally, we also demonstrate that the temporal developments of the wave profiles will depend

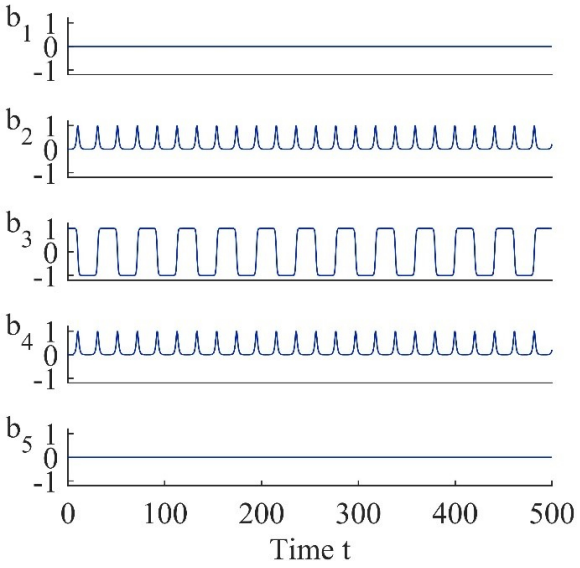

FIG. 15. An example of partial or minimal transfer of energy, as only modes of one triad A_2, A_3, A_4 are excited. The interaction coefficients have sign patterns as $s_1 = +1$, $s_2 = -1$, $s_{3a} = -1$, $s_{3b} = +1$, $s_4 = -1$, $s_5 = -1$.

critically on the magnitudes and sign patterns of the interaction coefficients. Hence the precise fluid mechanics input for wave resonance is crucially important.

It is instructive to point out the various possible extensions of the present work, as these discussions will highlight the merits as well as the limitations of this scope of studies. We have performed the nonlinear analysis for the case where the common member of the two triads is the parent wave. From the dispersion curves (Fig. 1), locating multiple triads where the common member is the daughter wave should be conceptually straightforward. The evolution equations for the nonlinear dynamics will follow patterns of Eq. (13) but with different combinations of quadratic nonlinearities. More importantly, the interaction coefficients will likely display another pattern of signs and magnitudes. As a result, different stability regimes and rogue wave features will emerge, but details will be reported in a future publication. In terms of the analytical context, a detailed comparison on the time invariants and characters of exact solutions between the two cases would be valuable [14,15].

Extensions to include configurations with the buoyancy frequency being spatially dependent should be attempted. A special case is N^2 [Eq. (4)] being the square of the hyperbolic secant [6]. Isolated triad resonance has been studied, but coupled triads ought to exist. This also will allow us to extend the consideration to the case of infinite or semi-infinite domains geometrically.

Nonlinear evolution equations should be derived for the two-layer shear flow case too, especially near the "mode interactions" region (Fig. 16). Both the "interfacial" and "surface" wave modes have nearly "flat" dispersion branches there, i.e., points of zero group velocities. Previous works discuss possible instability regime or an infinitely deep lower fluid, but do not address this exchange of identity region [49,50]. Comparisons and contrasts with existing results in the literature of internal waves would be a valuable exercise, especially on the intensively studied issue of parametric subharmonic instability [11–13]. Results from the present case of linearly stratified fluid display coefficients of opposite signs for each set of triad in the coupled cases, and hence "explosion" is unlikely. For other density profiles, these sign patterns will be addressed in future research works. Additional complications like critical layers may also arise [51].

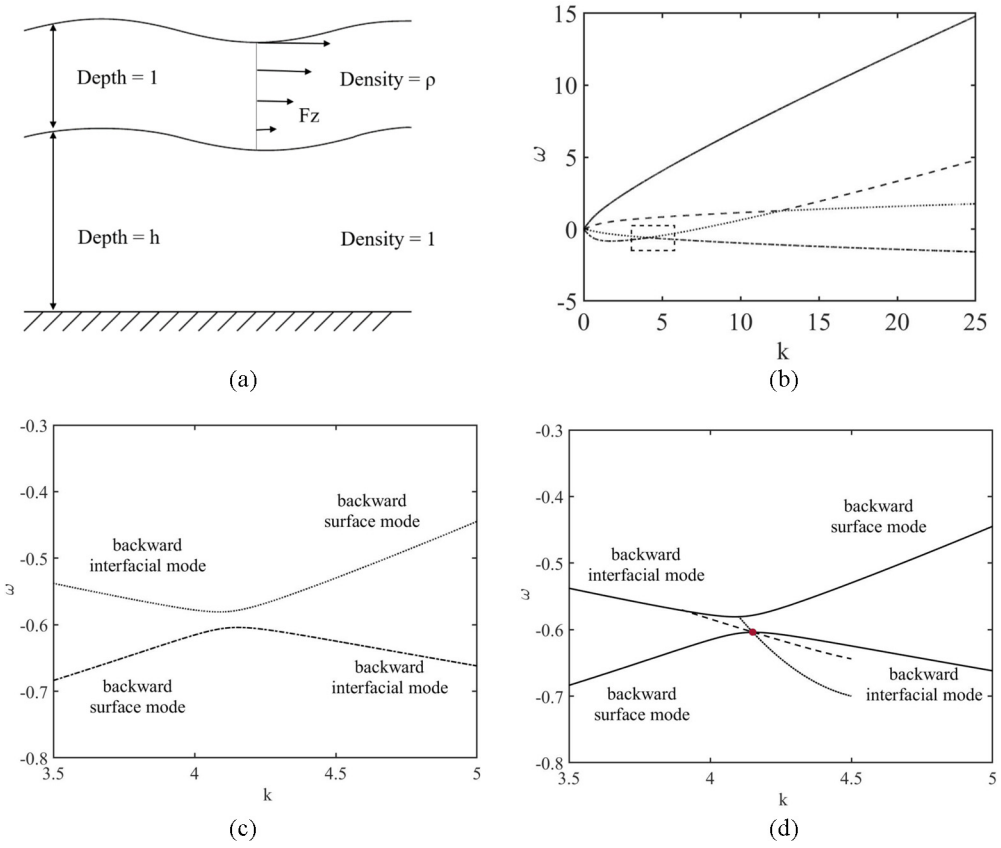

FIG. 16. (a) Schematic diagram of a two-layer fluid with shear flow in the upper layer. (b) Dispersion relation (angular frequency ω vs wave number k) for surface and interfacial waves for a moderate linear shear current $Fz, F = 0.4$. (c) "Close-up (zoom-in)" view of the region where the dispersion branches approach each other. (d) Schematic diagram of new coupled triad resonances by drawing the dispersion branches, "broken line" for the backward-moving interfacial mode and "dotted line" for the backward-moving surface mode, with a mode represented by a small circle as the common member of the coupled triads. Two distinct long waves (modes with small wave numbers) can participate in these resonances.

To apply the knowledge and trend here to a realistic ocean setting, we have to adjust the values of the wave number, buoyancy frequency, and channel depth utilized in this theoretical framework to relevant values in physical oceanography. The effects of shear currents, density stratification, and perhaps topography can be properly assessed [10,11,14,15,52]. Other issues of engineering significance, e.g., hydroelastic effects [53] and bathymetry [54], can be incorporated. We look forward to studying all these exciting directions for multiple triads, Fermi-Pasta-Ulam-Tsingou recurrence, and interaction phenomena for internal waves [36,55,56–58].

ACKNOWLEDGMENT

Partial financial support has been provided by the Research Grants Council General Research Fund Contract No. HKU17200718.

APPENDIX A: NONLINEAR EVOLUTION OF TRIADS

The interaction coefficients can be computed by applying the Fredholm alternative theorem to the second-order perturbation expansion of the equations of motion. Quadratic nonlinearities and slow time evolution constitute the main ingredients. For a resonance involving $k_3 = k_1 + k_5$, $\omega_3 = \omega_1 + \omega_5$ [Eq. (1)], we term the k_3 and the k_1/k_5 modes as the parent and daughter modes, respectively. We give examples of the formulation for quadratic nonlinearities involving combinations of "parent plus daughter" and "two daughters." The remaining coefficients can be deduced by cyclic changes of subscripts and superscripts.

We employ the symbols $\mathcal{H}_0$, $\mathcal{H}_1$, $\mathcal{H}_2$ to denote the quadratic nonlinearities arising from the incompressible condition, x-momentum, and z-momentum equations of motion. We then add superscripts to represent the wave pairs responsible for the particular interactions. Hence (1, 5) stand for interaction of mode 1 and mode 5 in generating mode 3 according to Eq. (1).

For interactions arising from two daughters mode k_1 and k_5, the nonlinearities are

$$\begin{aligned}
\mathcal{H}_0^{(1,5)} &= u^{(1)}\rho^{(5)}ik_5 + u^{(5)}\rho^{(1)}ik_1 + v^{(1)}(\rho^{(5)})_z + v^{(5)}(\rho^{(1)})_z,\\
\mathcal{H}_1^{(1,5)} &= u^{(1)}u^{(5)}ik_5 + u^{(5)}u^{(1)}ik_1 + v^{(1)}(u^{(5)})_z + v^{(5)}(u^{(1)})_z,\\
\mathcal{H}_2^{(1,5)} &= u^{(1)}v^{(5)}ik_5 + u^{(5)}v^{(1)}ik_1 + v^{(1)}(v^{(5)})_z + v^{(5)}(v^{(1)})_z,
\end{aligned} \tag{A1}$$

where u, v, ρ stand for the linear, first-order x velocity, z velocity and density, with no subscripts and/or superscripts to minimize the complexity of notations.

For interactions arising from a parent wave k_3 and a daughter mode k_5, the nonlinearities are

$$\begin{aligned}
\mathcal{H}_1^{(3,5)} &= u^{(3)}[ik_5u^{(5)}]^* + [u^{(5)}]^*[ik_3u^{(3)}] + v^{(3)}\left[u_z^{(5)}\right]^* + [v^{(5)}]^*u_z^{(3)},\\
\mathcal{H}_2^{(3,5)} &= u^{(3)}[ik_5v^{(5)}]^* + [u^{(5)}]^*[ik_3v^{(3)}] + v^{(3)}\left[v_z^{(5)}\right]^* + [v^{(5)}]^*v_z^{(3)},\\
\mathcal{H}_0^{(3,5)} &= u^{(3)}[ik_5\rho^{(5)}]^* + [u^{(5)}]^*[ik_3\rho^{(3)}] + v^{(3)}\left[\rho_z^{(5)}\right]^* + [v^{(5)}]^*\rho_z^{(3)}.
\end{aligned} \tag{A2}$$

For a generalized interaction involving daughter modes, k_m and k_n, the nonlinearities are

$$\begin{aligned}
\mathcal{H}_0^{(m,n)} &= u^{(m)}[ik_n\rho^{(n)}] + [u^{(n)}][ik_m\rho^{(m)}] + v^{(m)}\left[\rho_z^{(n)}\right] + [v^{(n)}]\rho_z^{(m)},\\
\mathcal{H}_1^{(m,n)} &= u^{(m)}[ik_nu^{(n)}] + [u^{(n)}][ik_mu^{(m)}] + v^{(m)}\left[u_z^{(n)}\right] + [v^{(n)}]u_z^{(m)},\\
\mathcal{H}_2^{(m,n)} &= u^{(m)}[ik_nv^{(n)}] + [u^{(n)}][ik_mv^{(m)}] + v^{(m)}\left[v_z^{(n)}\right] + [v^{(n)}]v_z^{(m)},
\end{aligned}$$

where the linear horizontal (vertical) velocities, density are

$$u^{(m)} = \frac{i}{k_m}(\phi_m)_zB_m, \quad v^{(m)} = \phi_mB_m, \quad \rho^{(m)} = \frac{i}{k_m}\frac{\bar{\rho}_z\phi_m}{U - c_m}B_m,$$

The eigenfunction ϕ_m satisfies the Taylor-Goldstein equation [Eq. (3)].

To evaluate a typical interaction coefficient like r_1 given in Eq. (13a), calculations involving the Fredholm alternative theorem give

$$r_1 = \frac{r_{1n}}{r_{1d}}, \quad r_{1n} = \int_0^H \left[\frac{1}{i} \frac{\partial \mathcal{H}_1^{(3,5)}}{\partial z} + \frac{1}{i} \frac{g}{\bar{\rho}(z)} \frac{\mathcal{H}_0^{(3,5)}}{(U - c_1)} - k_1 \mathcal{H}_2^{(3,5)} \right] \phi_1 dz,$$
$$r_{1d} = \frac{1}{k_1} \int_0^H \left[\frac{2N^2}{(U - c_1)^2} - \frac{U_{zz}}{U - c_1} \right] \phi_1^2 dz. \tag{A3}$$

One can easily write formulas like

$$r_{jn} = \int_0^H \left[\frac{1}{i} \frac{\partial \mathcal{H}_1^{(m,n)}}{\partial z} + \frac{1}{i} \frac{g}{\bar{\rho}(z)} \frac{\mathcal{H}_0^{(m,n)}}{(U - c_j)} - k_j \mathcal{H}_2^{(m,n)} \right] \phi_j dz,$$
$$r_{jd} = \frac{1}{k_j} \int_0^H \left[\frac{2N^2}{(U - c_j)^2} - \frac{U_{zz}}{U - c_j} \right] \phi_j^2 dz,$$

for other types of interactions.

APPENDIX B: EFFECTS OF THE BUOYANCY FREQUENCY N_0

For a stratified fluid of constant buoyancy frequency N_0 within a channel of depth H, the interaction coefficient r_j [Eq. (13)] will be proportional to the square of N_0. This can be readily demonstrated analytically. As example, take r_1 of Eq. (A3). As the phase speed c_1 is proportional to N_0 for the case of no shear $[U(y) = 0]$, N_0 will be eliminated in the first term in the integrand. As a result, r_{1d} will be independent of the buoyancy frequency N_0.

For the numerator, the integral of the terms in connection with ${\mathcal{H}_1}^{(3,5)}$, ${\mathcal{H}_2}^{(3,5)}$ will be zero, as expressions like (l, m, n being integers)

$$\int_0^H \sin\left(\frac{l\pi z}{H}\right) \sin\left(\frac{m\pi z}{H}\right) \cos\left(\frac{n\pi z}{H}\right) dz = 0$$

are involved. Finally, the nonzero contribution comes from ${\mathcal{H}_0}^{(3,5)}$, which can be reduced to an expression proportional to the square of the buoyancy frequency. The assertion is thus established. The feature is also verified numerically by our computer codes.

APPENDIX C: NEW INSTABILITY DUE TO COUPLING

The linearized stability equations arising from small disturbances imposed on plane waves are

$$\rho_1 \rho_1'(-i\zeta_1) + \rho_1 \frac{\partial \rho_1'}{\partial \tau} + c_{g1}\left(\rho_1 \rho_1' i\xi_1 + \rho_1 \frac{\partial \rho_1'}{\partial \hat{x}}\right) = i r_1 \rho_3 \rho_5 [\rho_3' + (\rho_5')^*],$$
$$\rho_2 \rho_2'(-i\zeta_2) + \rho_2 \frac{\partial \rho_2'}{\partial \tau} + c_{g2}\left(\rho_2 \rho_2' i\xi_2 + \rho_2 \frac{\partial \rho_2'}{\partial \hat{x}}\right) = i r_2 \rho_3 \rho_4 [\rho_3' + (\rho_4')^*],$$
$$i\rho_3 \rho_3'(-i\zeta_3) + i\rho_3 \frac{\partial \rho_3'}{\partial \tau} + c_{g3}\left((i\rho_3 \rho_3')(i\xi_3) + i\rho_3 \frac{\partial \rho_3'}{\partial \hat{x}}\right) = r_{3a} \rho_1 \rho_5 (\rho_1' + \rho_5') + r_{3b} \rho_2 \rho_4 (\rho_2' + \rho_4'),$$

$$\rho_4\rho_4'(-i\zeta_4)+\rho_4\frac{\partial\rho_4'}{\partial\tau}+c_{g4}\left(\rho_4\rho_4'i\xi_4+\rho_4\frac{\partial\rho_4'}{\partial\hat{x}}\right)=ir_4\rho_3\rho_2[(\rho_2')^*+\rho_3'],$$
$$\rho_5\rho_5'(-i\zeta_5)+\rho_5\frac{\partial\rho_5'}{\partial\tau}+c_{g5}\left(\rho_5\rho_5'i\xi_5+\rho_5\frac{\partial\rho_5'}{\partial\hat{x}}\right)=ir_5\rho_3\rho_5[\rho_3'+(\rho_1')^*],$$

By separating into real and imaginary parts, we obtain

$$\zeta_1\rho_1Q_1+\rho_1\frac{\partial P_1}{\partial\tau}+c_{g1}\left(-\xi_1\rho_1Q_1+\rho_1\frac{\partial P_1}{\partial\hat{x}}\right)+r_1\rho_3\rho_5(Q_3-Q_5)=0,$$
$$-i\zeta_1\rho_1P_1+i\rho_1\frac{\partial Q_1}{\partial\tau}+c_{g1}\left(i\xi_1\rho_1P_1+i\rho_1\frac{\partial Q_1}{\partial\hat{x}}\right)-ir_1\rho_3\rho_5(P_3+P_5)=0,$$
$$\zeta_2\rho_2Q_2+\rho_2\frac{\partial P_2}{\partial\tau}+c_{g2}\left(-\xi_2\rho_2Q_2+\rho_2\frac{\partial P_2}{\partial\hat{x}}\right)+r_2\rho_3\rho_4(Q_3-Q_4)=0,$$
$$-i\zeta_2\rho_2P_2+i\rho_2\frac{\partial Q_2}{\partial\tau}+c_{g2}\left(i\xi_2\rho_2P_2+i\rho_2\frac{\partial Q_2}{\partial\hat{x}}\right)-ir_2\rho_3\rho_4(P_3+P_4)=0,$$
$$\zeta_3\rho_3P_3-\rho_3\frac{\partial Q_3}{\partial\tau}+c_{g3}\left(-\xi_3\rho_3P_3-\rho_3\frac{\partial Q_3}{\partial\hat{x}}\right)-r_{3a}\rho_1\rho_5(P_1+P_5)-r_{3b}\rho_2\rho_4(P_2+P_4)=0,$$
$$i\zeta_3\rho_3Q_3+i\rho_3\frac{\partial P_3}{\partial\tau}+c_{g3}\left(-i\xi_3\rho_3Q_3+i\rho_3\frac{\partial P_3}{\partial\hat{x}}\right)-ir_{3a}\rho_1\rho_5(Q_1+Q_5)-ir_{3b}\rho_2\rho_4(Q_2+Q_4)=0,$$
$$\zeta_4\rho_4Q_4+\rho_4\frac{\partial P_4}{\partial\tau}+c_{g4}\left(-\xi_4\rho_4Q_4+\rho_4\frac{\partial P_4}{\partial\hat{x}}\right)+r_4\rho_3\rho_2(Q_3-Q_2)=0,$$
$$-i\zeta_4\rho_4P_4+i\rho_4\frac{\partial Q_4}{\partial\tau}+c_{g4}\left(i\xi_4\rho_4P_4+i\rho_4\frac{\partial Q_4}{\partial\hat{x}}\right)-ir_4\rho_3\rho_2(P_3+P_2)=0,$$
$$-i\zeta_5\rho_5P_5+i\rho_5\frac{\partial Q_5}{\partial\tau}+c_{g5}\left(i\xi_5\rho_5P_5+i\rho_5\frac{\partial Q_5}{\partial\hat{x}}\right)-ir_5\rho_3\rho_1(P_3+P_1)=0,$$
$$\zeta_5\rho_5Q_5+\rho_5\frac{\partial P_5}{\partial\tau}+c_{g5}\left(-\xi_5\rho_5Q_5+\rho_5\frac{\partial P_5}{\partial\hat{x}}\right)+r_5\rho_3\rho_1(Q_3-Q_1)=0.$$

After the normal mode separation of Eq. (14), the formulation is reduced to a matrix form:

$$A\begin{pmatrix}p_1\\p_2\\p_3\\p_4\\p_5\\q_1\\q_2\\q_3\\q_4\\q_5\end{pmatrix}=0,$$

where A is

$$A = \begin{pmatrix}
i\rho_1(-\Omega+Kc_{g1}) & 0 & 0 & 0 & 0 & -r_1\rho_3\rho_5 & 0 & r_1\rho_3\rho_5 & 0 & -r_1\rho_3\rho_5 \\
r_1\rho_3\rho_5 & 0 & -r_1\rho_3\rho_5 & 0 & -r_1\rho_3\rho_5 & i\rho_1(-\Omega+Kc_{g1}) & 0 & 0 & 0 & 0 \\
0 & i\rho_2(-\Omega+Kc_{g2}) & 0 & 0 & 0 & 0 & -r_2\rho_3\rho_4 & r_2\rho_3\rho_4 & -r_2\rho_3\rho_4 & 0 \\
0 & r_2\rho_3\rho_4 & -r_2\rho_3\rho_4 & -r_2\rho_3\rho_4 & 0 & 0 & i\rho_2(-\Omega+Kc_{g2}) & 0 & 0 & 0 \\
-r_{3a}\rho_1\rho_5 & -r_{3b}\rho_2\rho_4 & r_{3a}\rho_1\rho_5+r_{3b}\rho_2\rho_4 & -r_{3b}\rho_2\rho_4 & -r_{3a}\rho_1\rho_5 & 0 & 0 & i\rho_3(\Omega-Kc_{g3}) & 0 & 0 \\
0 & 0 & i\rho_3(-\Omega+Kc_{g3}) & 0 & 0 & -r_{3a}\rho_1\rho_5 & -r_{3b}\rho_2\rho_4 & r_{3a}\rho_1\rho_5+r_{3b}\rho_2\rho_4 & -r_{3b}\rho_2\rho_4 & -r_{3a}\rho_1\rho_5 \\
0 & 0 & 0 & i\rho_4(-\Omega+Kc_{g4}) & 0 & 0 & -r_4\rho_3\rho_2 & r_4\rho_3\rho_2 & -r_4\rho_3\rho_2 & 0 \\
0 & -r_4\rho_3\rho_2 & -r_4\rho_3\rho_2 & r_4\rho_3\rho_2 & 0 & -r_5\rho_3\rho_1 & 0 & 0 & i\rho_4(-\Omega+Kc_{g4}) & 0 \\
0 & 0 & 0 & 0 & i\rho_5(-\Omega+Kc_{g5}) & 0 & 0 & r_5\rho_3\rho_1 & 0 & -r_5\rho_3\rho_1 \\
-r_5\rho_3\rho_1 & 0 & -r_5\rho_3\rho_1 & 0 & r_5\rho_3\rho_1 & 0 & 0 & 0 & 0 & i\rho_5(-\Omega+Kc_{g5})
\end{pmatrix}.$$

For the purpose of comparison, the corresponding matrices for the triad modes (1, 5, 3) and triad modes (2, 4, 3) are given by

$$A_1 = \begin{pmatrix} i\rho_1(-\Omega+Kc_{g1}) & 0 & 0 & -r_1\rho_3\rho_5 & r_1\rho_3\rho_5 & -r_1\rho_3\rho_5 \\ r_1\rho_3\rho_5 & -r_1\rho_3\rho_5 & -r_1\rho_3\rho_5 & i\rho_1(-\Omega+Kc_{g1}) & 0 & 0 \\ -r_{3a}\rho_1\rho_5 & r_{3a}\rho_1\rho_5 & -r_{3a}\rho_1\rho_5 & 0 & i\rho_3(\Omega-Kc_{g3}) & 0 \\ 0 & i\rho_3(-\Omega+Kc_{g3}) & 0 & -r_{3a}\rho_1\rho_5 & r_{3a}\rho_1\rho_5 & -r_{3a}\rho_1\rho_5 \\ 0 & 0 & i\rho_5(-\Omega+Kc_{g5}) & -r_5\rho_3\rho_1 & r_5\rho_3\rho_1 & -r_5\rho_3\rho_1 \\ -r_5\rho_3\rho_1 & -r_5\rho_3\rho_1 & r_5\rho_3\rho_1 & 0 & 0 & i\rho_5(-\Omega+Kc_{g5}) \end{pmatrix}$$

and

$$A_2 = \begin{pmatrix} i\rho_2(-\Omega+Kc_{g2}) & 0 & 0 & -r_2\rho_3\rho_4 & r_2\rho_3\rho_4 & -r_2\rho_3\rho_4 \\ r_2\rho_3\rho_4 & -r_2\rho_3\rho_4 & -r_2\rho_3\rho_4 & i\rho_2(-\Omega+Kc_{g2}) & 0 & 0 \\ -r_{3b}\rho_2\rho_4 & r_{3b}\rho_2\rho_4 & -r_{3b}\rho_2\rho_4 & 0 & i\rho_3(\Omega-Kc_{g3}) & 0 \\ 0 & i\rho_3(-\Omega+Kc_{g3}) & 0 & -r_{3b}\rho_2\rho_4 & r_{3b}\rho_2\rho_4 & -r_{3b}\rho_2\rho_4 \\ 0 & 0 & i\rho_4(-\Omega+Kc_{g4}) & -r_4\rho_3\rho_2 & r_4\rho_3\rho_2 & -r_4\rho_3\rho_2 \\ -r_4\rho_3\rho_2 & -r_4\rho_3\rho_2 & r_4\rho_3\rho_2 & 0 & 0 & i\rho_4(-\Omega+Kc_{g4}) \end{pmatrix}.$$

APPENDIX D: GOVERNING EQUATION FOR THE ADDITIONAL INVARIANT

Regarding the calculation for the additional invariant of Eq. (23), we define a new expression

$$f(X) = \frac{s_1 b_5}{b_1} + \frac{s_5 b_1}{b_5}. \tag{D1}$$

By taking the square of Eq. (21), we obtain

$$\frac{b_4^2}{b_2^2} + 2s_2 s_4 + \frac{b_2^2}{b_4^2} = f^2(X). \tag{D2}$$

Straightforward algebra now gives

$$b_2^4 + \left[2s_2 s_4 b_4^2 - f^2(X) b_4^2\right] b_2^2 + b_4^4 = 0,$$

or

$$b_2^2 = \frac{[f^2(X) - 2s_2 s_4] \pm \sqrt{[f^2(X) - 2s_2 s_4]^2 - 4}}{2} b_4^2.$$

Finally, we arrive at

$$\begin{aligned}
Y &= \frac{Y_n}{Y_d}, \\
Y_n &= \frac{1}{2} b_4^2(0)\{[f^2(X) - 2s_2 s_4] \pm \sqrt{[f^2(X) - 2s_2 s_4]^2 - 4}\} - b_2^2(0), \\
Y_d &= \frac{1}{s_2} - \frac{1}{2s_4}\{[f^2(X) - 2s_2 s_4] \pm \sqrt{[f^2(X) - 2s_2 s_4]^2 - 4}\}, \\
f^2(X) &= \frac{\frac{X}{s_5} + b_5^2(0)}{\frac{X}{s_1} + b_1^2(0)} + \frac{\frac{X}{s_1} + b_1^2(0)}{\frac{X}{s_5} + b_5^2(0)} + 2s_1 s_5.
\end{aligned} \tag{D3}$$

The actual evolution equation of the amplitude is given by

$$\left(\frac{dX}{d\tau}\right)^2 = 4b_1^2 b_3^2 b_5^2 \cos^2\theta = 4b_1^2 b_3^2 b_5^2 - 4\Gamma_1^2,$$

or

$$\left(\frac{dX}{d\tau}\right)^2 = 4\left[\frac{X}{s_1} + b_1^2(0)\right]\left[\frac{X}{s_5} + b_5^2(0)\right]\left[\frac{(X+Y)}{s_3} + b_3^2(0)\right] - 4\Gamma_1^2, \tag{D4}$$

where Y is defined via Eq. (D3).

APPENDIX E: TWO-LAYER FLUID WITH A SHEAR CURRENT

As another example of coupled triads with all five waves moving in the same direction, a two-layer fluid with a linear shear current in the upper layer is considered. The upper (lower) fluid has a depth of unity (h) and density ρ (unity) respectively (Fig. 16). A linear shear current Fz is assumed to be established in the upper layer. With g being gravity, the linear dispersion relation for angular frequency ω and wave number k can be computed by the standard kinematic and dynamic boundary

conditions:

$$\omega^4[\cosh(k)\coth(kh)+\rho\sinh(k)]+\omega^3[-2Fk\cosh(k)\coth(kh)-2Fk\rho\sinh(k)$$
$$+F\coth(kh)\sinh(k)]+\omega^2[-gk\cosh(k)+F^2k\rho\cosh(k)+F^2k^2\cosh(k)\coth(kh)$$
$$-F^2\rho\sinh(k)+F^2k^2\rho\sinh(k)-F^2k\coth(kh)\sinh(k)-gk\coth(kh)\sinh(k)]$$
$$+\omega[-Fgk\sinh(k)+2Fgk^2\cosh(k)-2Fgk^2\rho\cosh(k)-F^3k^2\rho\cosh(k)+F^3k\rho\sinh(k)$$
$$+2Fgk\rho\sinh(k)]+gk^2[F^2(\sinh(k)-k\cosh(k))+g\sinh(k)](1-\rho)=0. \quad \text{(E1)}$$

There will in general be two surface modes and two interfacial modes. With the presence of a current, eventually sufficiently short waves cannot propagate upstream. The dispersion branch for the backward surface mode bends due to the current and comes close to that of the backward interfacial mode. There is an "exchange of identity" and the branches never actually intersect (Fig. 16) [1].

There is a substantial literature on such two-layer shear flows, including the case of triad resonance [32]. We just highlight the remarkable feature at this exchange of identity point. Standard graphical construction of triad resonance will reveal the existence of coupled triads with two modes of small wave numbers (Fig. 16), due to the small size of the "gap." 'Long wave–short wave resonance" with multiple short waves and one common long wave has been studied in the literature [33,34]. The present configuration suggests one scenario with two long wave modes, and will open up exciting directions for such long wave dynamics to be pursued in future studies [35].

[1] A. D. D. Craik, *Wave Interactions and Fluid Flows* (Cambridge University Press, Cambridge, 1985).
[2] C. C. Mei, *The Applied Dynamics of Ocean Surface Waves* (World Scientific, Singapore, 1989).
[3] O. M. Phillips, Wave interactions–the evolution of an idea, J. Fluid Mech. **106**, 215 (1981).
[4] B. K. Campbell and Y. Liu, Sub-harmonic resonant wave interactions in the presence of a linear interfacial instability, Phys. Fluids **26**, 082107 (2014).
[5] M.-R. Alam, A new triad resonance between co-propagating surface and interfacial waves, J. Fluid Mech. **691**, 267 (2012).
[6] N. T. Hung and S. A. Maslowe, Interaction of internal waves in a continuous thermocline model, Austral. Math. Soc. Ser. B **25**, 94 (1983).
[7] G. Michel, Three-wave interactions among surface gravity waves in a cylindrical container, Phys. Rev. Fluids **4**, 012801(R) (2019).
[8] A. Cazaubiel, F. Haudin, E. Falcon, and M. Berhanu, Forced three-wave interactions of capillary-gravity surface waves, Phys. Rev. Fluids **4**, 074803 (2019).
[9] T. Dauxois, S. Joubaud, P. Odier, and A. Venaille, Instabilities of internal gravity wave beams, Annu. Rev. Fluid Mech. **50**, 131 (2018).
[10] B. R. Sutherland and R. Jefferson, Triad resonant instability of horizontally periodic internal modes, Phys. Rev. Fluids **5**, 034801 (2020).
[11] H. H. Karimi and T. R. Akylas, Near-inertial parametric subharmonic instability of internal wave beams, Phys. Rev. Fluids **2**, 074801 (2017).
[12] D. Varma and M. Mathur, Internal wave resonant triads in finite-depth non-uniform stratifications, J. Fluid Mech. **824**, 286 (2017).
[13] D. Olbers, F. Pollmann, and C. Edena, On PSI interactions in internal gravity wave fields and the decay of baroclinic tides, J. Phys. Oceanogr. **50**, 751 (2020).
[14] B. Fan and T. R. Akylas, Effect of background mean flow on PSI of internal wave beams, J. Fluid Mech. **869**, R1 (2019).
[15] K. Obuse and M. Yamada, Three-wave resonant interactions and zonal flows in two-dimensional Rossby-Haurwitz wave turbulence on a rotating sphere, Phys. Rev. Fluids **4**, 024601 (2019).

[16] D. J. Kaup, A. Reiman, and A. Bers, Space-time evolution of nonlinear three-wave interactions. I. Interaction in a homogeneous medium, Rev. Mod. Phys. **51**, 275 (1979).
[17] H. Wilhelmsson and V. P. Pavlenko, Five wave interaction - a possibility for enhancement of optical or microwave radiation by nonlinear coupling to explosively unstable plasma waves, Phys. Scr. **7**, 213 (1973).
[18] A. Z. Loesch and A. Domaracki, Dynamics of N resonantly interacting baroclinic waves, J. Atmos. Sci. **34**, 22 (1977).
[19] W. Kim and B. J. West, Chaotic properties of internal wave triad interactions, Phys. Fluids **9**, 632 (1997).
[20] F. J. Romeiras, Double three-wave interaction of four waves: Lax representation and exact solutions, J. Math. Phys. **35**, 4757 (1994).
[21] S. R. Lopes and F. B. Rizzato, Nonintegrable dynamics of the triplet-triplet spatiotemporal interaction, Phy. Rev. E **60**, 5375 (1999).
[22] C. R. Menyuk, H. H. Chen, and Y. C. Lee, Restricted multiple three-wave interactions: Integrable cases of this system and other related systems, J. Math. Phys. **24**, 1073 (1983).
[23] F. Verheest, Integrability of restricted multiple three-wave interactions. II. Coupling constants with ratios 1 and 2, J. Math. Phys. **29**, 2197 (1988).
[24] E. Kartashova and V. S. L'vov, Cluster dynamics of planetary waves, Europhys. Lett. **83**, 50012 (2008).
[25] M. D. Bustamante and E. Kartashova, Effect of the dynamical phases on the nonlinear amplitudes' evolution, Europhys. Lett. **85**, 34002 (2009).
[26] D. I. Pullin and R. H. J. Grimshaw, Interfacial progressive gravity waves in a two-layer shear flow, Phys. Fluids **26**, 1731 (1983).
[27] Q. Pan, R. H. J. Grimshaw, and K. W. Chow, Modulation instability and rogue waves for shear flows with a free surface, Phys. Rev. Fluids **4**, 084803 (2019).
[28] T. D. Drivas and S. Wunsch, Triad resonance between gravity and vorticity waves in vertical shear, Ocean Model. **103**, 87 (2016).
[29] R. Raj and A. Guha, On Bragg resonances and wave triad interactions in two-layered shear flows, J. Fluid Mech. **867**, 482 (2019).
[30] Y. Kivshar and G. Agrawal, *The Optical Solitons*: *From Fibers to Photonic Crystals* (Academic Press, San Diego, 2003).
[31] A. K. Liu and D. J. Benney, The evolution of nonlinear wave trains in stratified shear flows, Stud. Appl. Math. **64**, 247 (1981).
[32] F. de Melo Viríssimo and P. A. Milewski, Nonlinear stability of two-layer shallow water flows with a free surface, Proc. R. Soc. A **476**, 20190594 (2020).
[33] Y. C. Ma, The resonant interaction among long and short waves, Wave Motion **3**, 257 (1981).
[34] H. N. Chan, E. Ding, D. J. Kedziora, R. Grimshaw, and K. W. Chow, Rogue waves for a long wave–short wave resonance model with multiple short waves, Nonlinear Dyn. **85**, 2827 (2016).
[35] H. N. Chan, R. H. J. Grimshaw, and K. W. Chow, Modeling internal rogue waves in a long wave-short wave resonance framework, Phys. Rev. Fluids **3**, 124801 (2018).
[36] F. Coppini and P. M. Santini, Fermi-Pasta-Ulam-Tsingou recurrence of periodic anomalous waves in the complex Ginzburg-Landau and in the Lugiato-Lefever equations, Phys. Rev. E **102**, 062207 (2020).
[37] G. P. Agrawal, Modulation Instability Induced by Cross-Phase Modulation, Phys. Rev. Lett. **59**, 880 (1987).
[38] M. Onorato, A. R. Osborne, and M. Serio, Modulational Instability in Crossing Sea States: A Possible Mechanism for the Formation of Freak Waves, Phys. Rev. Lett. **96**, 014503 (2006).
[39] R. Grimshaw, E. Pelinovsky, T. Taipova, and A. Sergeeva, Rogue internal waves in the ocean: Long wave model, Eur. Phys. J. Special Topics **185**, 195 (2010).
[40] A. Ankiewicz and M. Bokaeeyan, Integral relations for rogue wave formations of Gardner equation, Nonlinear Dyn. **99**, 2939 (2020).
[41] T. Talipova, O. Kurkina, A. Kurkin, E. Didenkulov, and E. Pelinovsky, Internal wave breathers in the slightly stratified fluid, Microgravity Sci. Technol. **32**, 69 (2020).
[42] M. Onorato, S. Residori, U. Bortolozzo, A. Montina, and F. T. Arecchi, Rogue waves and their generating mechanisms in different physical contexts, Phys. Rep. **528**, 47 (2013).

[43] F. Baronio, M. Conforti, A. Degasperis, and S. Lombardo, Rogue Waves Emerging from the Resonant Interaction of Three Waves, Phys. Rev. Lett. **111**, 114101 (2013).
[44] A. Chabchoub, N. Hoffmann, M. Onorato, and N. Akhmediev, Super Rogue Waves: Observation of a Higher-Order Breather in Water Waves, Phys. Rev. X **2**, 011015 (2012).
[45] M. L. McAllister, S. Draycott, T. A. A. Adcock, P. H. Taylor, and T. S. van den Bremer, Laboratory recreation of the Draupner wave and the role of breaking in crossing seas, J. Fluid Mech. **860**, 767 (2019).
[46] F. Fedele, J. Brennan, S. P. de León, J. Dudley, and F. Dias, Real world ocean rogue waves explained without the modulational instability, Sci. Rep. **6**, 27715 (2016).
[47] E. L. Geist, Effect of dynamical phase on the resonant interaction among tsunami edge wave modes, Pure Appl. Geophys. **175**, 1341 (2018).
[48] Y. Liang, A. Zareei, and M.-R. Alam, Inherently unstable internal gravity waves due to resonant harmonic generation, J. Fluid Mech. **811**, 400 (2017).
[49] I. Brevik and H. Sund, The Kelvin-Helmholtz instability for surface waves in currents of uniform vorticity, Phys. Fluids A **5**, 1644 (1993).
[50] A. I. Baumstein, Modulation of gravity waves with shear in water, Stud. Appl. Math. **100**, 365 (1998).
[51] J. M. Becker and R. H. J. Grimshaw, Explosive resonant triads in a continuously stratified shear-flow, J. Fluid Mech. **257**, 219 (1993).
[52] J. Thomas and R. Yamada, An amplitude equation for surface gravity wave-topography interactions, Phys. Rev. Fluids **3**, 124802 (2018).
[53] L. Deike, M. Berhanu, and E. Falcon, Experimental observation of hydroelastic three-wave interactions, Phys. Rev. Fluids **2**, 064803 (2017).
[54] K. A. Belibassakis, B. Simon, J. Touboul, and V. Rey, A coupled-mode model for water wave scattering by vertically sheared currents in variable bathymetry regions, Wave Motion **74**, 73 (2017).
[55] R. N. Ibragimov, S. Bakhtiyarov, and P. Zweigart, Correlation between three-dimensional sine sweep dynamics vibration testing and resonantly interacting internal gravity wave field, Math. Model. Nat. Phenom. **12**, 62 (2017).
[56] J. J. Liang, T. Du, X. M. Li, and M. He, Generation of mode-2 internal waves in a two-dimensional stratification by a mode-1 internal wave, Wave Motion **83**, 227 (2018).
[57] M. Bokaeeyan, A. Ankiewicz, and N. Akhmediev, Bright and dark rogue internal waves: The Gardner equation approach, Phys. Rev. E **99**, 062224 (2019).
[58] F. Hadadifard and J. D. Wright, Mass-in-mass lattices with small internal resonators, Stud. Appl. Math. **146**, 81 (2021).